DIPARTIMENTO DI MEDICINA DI PRECISIONE IN AREA MEDICA, CHIRURGICA E CRITICA (Me.Pre.C.C.)
Dottorato di ricerca in Oncologia e Chirurgia Sperimentali
Coordinatore: Prof. Antonio Russo

UNIVERSITÀ DEGLI STUDI DI PALERMO

Dottorato di ricerca in Oncologia e Chirurgia Sperimentali

DIPARTIMENTO DI MEDICINA DI PRECISIONE IN AREA MEDICA, CHIRURGICA E CRITICA

(Me.Pre.C.C.)

Functional characterization of mammalian and plant extracellular vesicles as systems for cancer treatment

Doctoral Dissertation of:

Nima RabieNezhad Ganji

Tutor:

Prof. Riccardo Alessandro

Co-Tutor:

Prof.ssa Stefania Raimondo

The Chair of the Doctoral Program:

Prof. Antonio Russo

2024 – XXXV° ciclo

INDEX

Abstract

In the last years, the field of nanomedicine and drug delivery has grown exponentially, providing new platforms to carry therapeutic agents into the target sites. Extracellular vesicles (EVs) are ready-to-use, biocompatible, and non-toxic nanoparticles that are revolutionizing the field of drug delivery. EVs are involved in cell-cell communication and mediate many physiological and pathological processes by transferring their bioactive cargo to target cells. Recently, nanovesicles from plants (PDNVs) have raised the interest of the scientific community due to their high yield and biocompatibility. This study aims to first evaluate whether PDNVs may be used as drug delivery systems. We isolated and characterized nanovesicles from tangerine juice (TNVs) that were comparable to mammalian EVs in size and morphology. TNVs carry the traditional EV marker HSP70 and, as demonstrated by metabolomic analysis, contain flavonoids, organic acids, and limonoids. TNVs were loaded with DDHD1-siRNA through electroporation, obtaining a loading efficiency of 13%. The DDHD1 gene encodes the phospholipase DDHD1 protein, which plays a vital role in lipid metabolism by hydrolyzing phospholipids into fatty acids and other lipophilic substances. Overexpression of DDHD1 has been linked to increased proliferation in colorectal cancer cells, suggesting its potential as a target for cancer therapies. We found that the DDHD1-siRNA TNV complexes were able to deliver DDHD1-siRNA to human colorectal cancer cells, inhibiting the target expression by about 60%. This study represents a proof of concept for the use of PDNVs as vehicles of RNA interference (RNAi) toward mammalian cells. More recently we tested whether the approach used with PDNVs can be applied also to mammalian vesicles, in particular to EVs purified from human embryonic kidney cells (HEK293T). We focused on loading onco-suppressor microRNAs, miR-146a and miR-199a, in EVs and to test the functionality of the complex on thyroid cancer cell lines. To increase the cell-specific targeting of the EV-miRNA complex, we decorated exosomes with Hyaluronic acid (HA), since cancer cells overexpress its receptor, CD44. Preliminary results suggest that the developed electroporation approach can be also used to load exogenous RNA in mammalian EVs; also, our findings suggest that the decoration of EV with HA may enhance the delivery efficiency of miRNAs to target cells.

CHAPTER 1

Background

1.1. Extracellular Vesicles

1.1.1. Overview and Definition

Extracellular vesicles (EVs) are lipoproteic structures released by cells in the extracellular space, contributing to intercellular communication. Recent research has shed light on their intricate nature and diverse functions. EVs are heterogeneous in size, from few nanometers to micrometers, and in the variety of molecules they can carry, including proteins, nucleic acids, and lipids. This sophisticated cargo can significantly influence the recipient cell phenotype. Understanding the complexities of these membrane-bound particles is an exciting frontier in the field of intercellular communication (1). EVs as mediators regulate cellular activities and have a significant impact on cancer progression and other diseases (2); also, EVs have multifaceted roles in action, which include immune modulation, tissue regeneration, spread and metastases of cancer, and neurological disorders (3). Cells adopt a regulated process to release EVs in response to external stimuli; as a result, their release shows remarkable compatibility with physiological and pathological conditions (4). A deep understanding of the function of EVs, and paying attention to their multifaceted roles, may lead to the transformation of EVs into a tool for drug delivery and disease diagnosis in medical science (5). The historical landscape of EVs reflects a journey from obscurity to recognition. At first, EVs were known as wastes and cellular debris that were not given much importance. With the emergence of diseases in the 20th century, researchers' attention to EVs increased. Studies in the field of EVs, including biogenesis pathways, cargo composition, and cell transport mechanisms changed our understanding of the importance of EVs in disease and health (6,7,8,9).

1.1.2. Isolation and Characterization

To fully understand EVs as a universal cell biological system and its translational applications, optimal techniques for their isolation and identification are required. Various isolation

techniques, like ultracentrifugation and size exclusion chromatography, are used depending on the source of EVs. Recent advancements in microfluidic-based isolation techniques and high-resolution imaging methods have enhanced EV analysis, crucial for understanding EVs and their applications. After extraction, EV characteristics are studied using techniques such as Transmission Electron Microscopy (TEM), Dynamic Light Scattering (DLS), and Nanoparticle Tracking Analysis (NTA). These methods provide valuable insights into EV biology and potential clinical applications (10,11).

1.2. Mammalian-Derived Vesicles

Mammalian-derived extracellular vesicles, like other sources of extracellular vesicle, act as vital mediators of intercellular communication and play pivotal roles in various physiological processes. These EVs include exosomes, microvesicles, and apoptotic bodies, each originating from distinct cellular pathways and carrying diverse biomolecules (12).

1.2.1. Characteristics and Composition

Extracellular vesicles carry a large number of biological molecules, thus influencing the recipient cell phenotype. These molecules include proteins, lipids, RNA, and cellular metabolites that represent the information of the cell of origin; therefore, the composition of EVs can vary depending on factors such as the cell type from which they are derived, the physiological state of the cell, and environmental stimuli. The composition of EVs can provide insights into their biogenesis, cargo sorting mechanisms, and potential roles in intercellular communication and disease processes. Studying the composition of EVs involves techniques such as proteomics, lipidomics, and RNA sequencing to identify and characterize the specific molecules contained within these vesicles. Through the transfer of genetic material such as microRNAs (miRNAs), messenger RNAs (mRNAs) and even DNA fragments, EVs can modulate gene expression in target cells, thereby affecting a variety of cellular processes from proliferation and differentiation to affect apoptosis and regulation of immune response (14). In addition, EV-mediated transport of growth factors, cytokines, and extracellular matrix components facilitates intercellular interactions essential for coordinating homeostasis and tissue regeneration in various physiological contexts, including wound healing and organ growth (15).

1.2.2. Exosomes

Exosomes, or exosome-like vesicles, are uniformly round, membrane-covered structures with a diameter of 30–150 nm (Figure 1A). Exosomes, essential mediators of intercellular

communication, are intricately formed through a highly regulated mechanism. This process primarily involves the endosomal sorting complexes required for transport (ESCRT) machinery, consisting of ESCRT-0, ESCRT-I, ESCRT-II, and ESCRT-III complexes, which orchestrate the sorting of specific cargo molecules into intraluminal vesicles (ILVs) within multivesicular bodies (MVBs). ESCRT-III, along with associated proteins like VPS4 and VTA1, facilitate membrane abscission and MVB maturation, ultimately leading to the release of ILVs as exosomes into the extracellular space. Alternatively, ceramide synthesis operates as an ESCRT-independent mechanism, promoting membrane curvature and ILV budding. Characterization of exosomes relies on identifying specific markers enriched in their membrane or cargo contents, such as tetraspanin proteins (e.g., CD9, CD63, CD81, CD82), Alix, Tsg101, as well as major histocompatibility complex (MHC) proteins and heat shock proteins (HSP) (Figure 1B). Understanding exosome biogenesis and molecular composition not only advances fundamental knowledge of intercellular communication but also offers promising avenues for diagnostic and therapeutic applications (13,16,17,18).

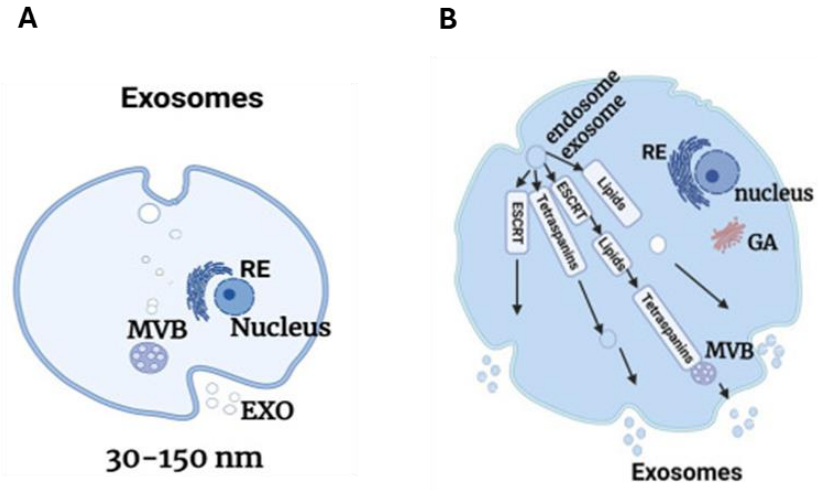

Figure 1. (A) Schematic illustration of the formation of exosome. (B) The molecular machinery of EXO biogenesis: schematization of the different pathways involved in EXO formation involving the ESCRT machinery, tetraspanins, and some lipids (Sall IM, 2023).

1.2.3 Microvesicles

Microvesicles (MVs) also called microparticles (MPs) are vesicles that bud by burgeoning from the plasma membrane and have a size of 50–100 nm or even more (Figure 2A). MVs biogenesis is a highly dynamic process orchestrated by various cellular components and signaling pathways. Central to this process is the regulation of intracellular calcium levels, which triggers cytoskeletal remodeling and membrane dynamics. Increased calcium concentrations activate enzymatic machinery that alter membrane phospholipid composition, leading to

phosphatidylserine externalization and membrane curvature, essential for MV release. Lipids like cholesterol and small GTPases, particularly members of the RHO family, along with their effectors and regulators, play critical roles in modulating membrane fluidity and cytoskeletal dynamics during MVs formation. Additionally, MVs release involves plasma membrane rupture facilitated by actin-myosin interactions and ATP-dependent contraction, with emerging evidence pointing to the involvement of regulatory mechanisms like the ESCRT machinery, ATP-dependent P2X receptor 7, and acid sphingomyelinase translocation (Figure 2B). (17,19).

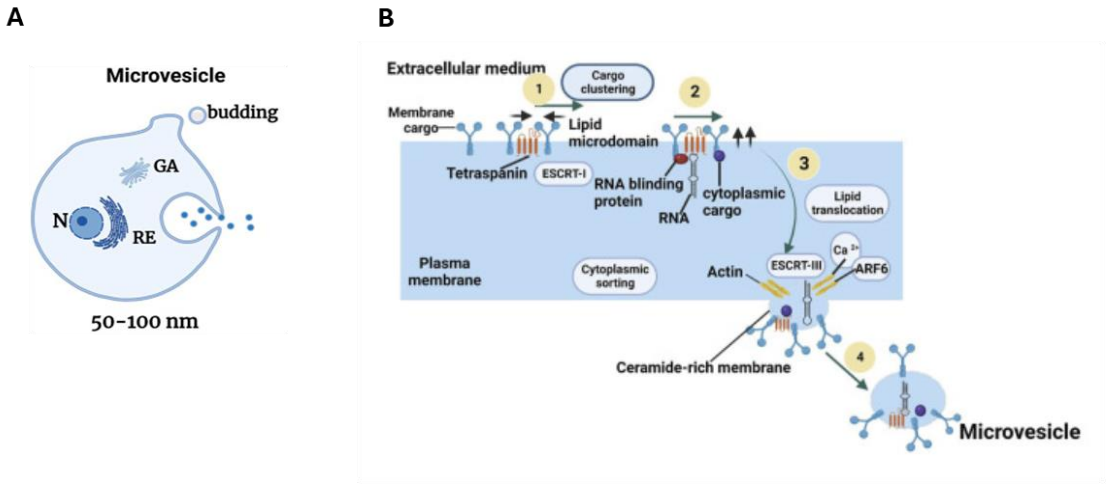

Figure 2. (A) Schematic illustration of the formation of Microvesicle. (B) ARF6: ADP-Ribosylation Factor 6; ESCRT: Endosomal Sorting Complex Required for Transport (Sall IM, 2023).

1.2.4. Apoptotic Bodies

Apoptotic bodies also called apoptosomes are vesicles with the dimension of 1–5 µm released by cells in apoptosis (Figure 3A). Apoptotic bodies, characterized by their larger size and distinct molecular markers, are formed as a result of cellular fragmentation during apoptosis, a crucial process in programmed cell death. This orchestrated mechanism involves the activation of intrinsic or extrinsic signaling pathways, leading to cellular demise and the eventual release of apoptotic bodies (Figure 3B). At the cellular level, apoptotic bodies are generated through actomyosin contractions, inducing membrane blebbing and subsequent membrane scission, liberating these vesicles into the extracellular environment. Alongside apoptotic bodies, smaller apoptotic vesicles are also produced, potentially representing a unique population of apoptotic extracellular vesicles with specific functional roles in intercellular communication and immune modulation. The intricate process of apoptotic vesicle formation highlights the complexity of apoptotic cell death and its influence on tissue homeostasis, inflammation, and immune responses. The release of apoptotic vesicles not only facilitates the clearance of apoptotic cells

but also enables communication with neighboring cells, affecting various physiological processes (20).

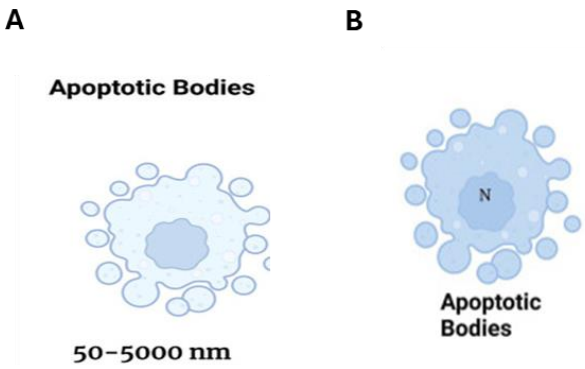

Figure 3. (A) Schematic illustration of the formation of Apoptotic Bodies. (B) Apoptotic body extrusion appears in the scheme and in sections of conventionally embedded apoptotic cells (Sall IM, 2023).

In line with the MISEV2023 recommendations, the traditional classification of extracellular vesicles (EVs) into exosomes, microvesicles, and apoptotic bodies has been revised. MISEV2023 suggests exercising caution when using biogenesis-based terms such as exosome, ectosome (microvesicle), and apoptotic bodies unless there is strong evidence for their specific subcellular origin. This caution arises from the overlapping size profiles and the absence of universal molecular markers that can definitively distinguish these subtypes. Traditionally, exosomes are defined as EVs derived from the endosomal pathway (multivesicular bodies), microvesicles (or ectosomes) as those that bud directly from the plasma membrane, and apoptotic bodies as large EVs released during programmed cell death. However, isolating pure populations of these vesicles is difficult, leading to potential mixtures in most preparations. To address this, MISEV2023 recommends using more descriptive terms based on physical characteristics, such as small EVs (sEVs) for particles under 200 nm and large EVs (lEVs) for particles over 200 nm, as well as biochemical composition or the conditions under which EVs were generated. This approach enhances clarity and accuracy in EV research and communication (21).

1.2.5. Biological Activities of Mammalian-EVs

Mammalian-derived vesicles have emerged as central players in the complex landscape of pathogenesis and disease progression, exerting profound effects in a range of medical conditions. In the context of various diseases, the disorder of EVs secretion and the altered levels of EVs in biological fluids are closely related to the pathogenesis and progression of several disorders, from neurodegenerative diseases to cancer and inflammatory diseases (22,23). Aberrant release

of EVs contributes to disease progression through multifaceted mechanisms, including modulation of cellular behavior, promotion of inflammatory responses, and modulation of immune responses (24). EVs play pivotal roles in shaping the cellular microenvironment and fostering disease-related phenotypes by transmitting information to neighboring cells. Furthermore, EVs derived from specific cell types often carry distinct sets of biomarkers reflecting the pathological state, which provide valuable insights into disease mechanisms and potential avenues for applications and provide diagnosis and prognosis (25). Understanding the roles of EVs in disease processes paves the way for the development of innovative strategies aimed at exploiting the diagnostic and therapeutic potential of these vesicles, thereby advancing precision medicine approaches, and improving patient outcomes (23,25).

1.3. Plant-Derived Vesicles

1.3.1. Origin and Biogenesis

Plant-derived nanovesicles (PDNVs) have gained increasing attention for their pivotal role in cellular communication and transport of biomolecules. According to Pinedo et al., (26) PDNVs can be classified into two main groups: plant extracellular vesicles (PEVs), isolated from an extracellular medium such as the apoplast, and plant-derived nanovesicles (PDNVs) isolated from a whole plant extraction such as juice and containing PEVs as well as other nanovesicles (27). The understanding of the formation and release of PDNVs is a critical aspect that still needs to be clarified. This knowledge presents opportunities for manipulating these processes for agricultural or therapeutic purposes, potentially revolutionizing practices in these domains (27,28). The intricate nature of PDNVs biogenesis involves multiple biomarkers and distinct pathways. Biomarkers like PENETRATION1 (PEN1), Tetraspanins, particularly TETRASPANIN 8/TETRASPANIN 9 (TET8/TET9), play a crucial role in biogenesis. The formation pathway of PDNVs shares similarities with exosomes, if associated with TET8 and/or TET9, they are produced by multivesicular bodies (MVBs). Moreover, an alternative pathway has been observed in EXPO (EXocyst-Positive Organelles), which appear as spherical double-membrane structures. Although resembling autophagosomes, which fuse with the plasma membrane and release membrane vesicles into the cell wall, they are considered exosomes secreted by EXPO (Figure 4). This discovery underscores the complexity and diversity of PDNVs' biogenesis pathways, emphasizing the need for further exploration to fully understand their roles and potential applications (29,30).

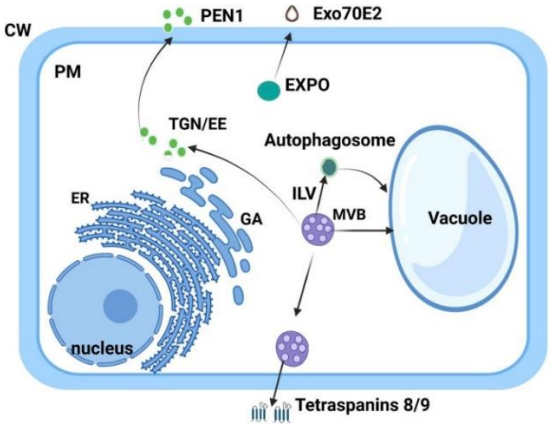

Figure 4. Biogenesis of exosomes in plant-derived nanovesicles (Sall IM, 2023).

1.3.2. Composition

PDNVs encompass a rich assortment of constituents including lipids, proteins, and nucleic acids (31). Lipids are known as essential components in nanovesicles. Analysis of different PDNVs shows different lipid compositions. Notably, galactosyl monoacylglycerol, phosphatidyl ethanolamine, and ceramide were found to be abundant in certain PDNVs. Lipid compounds are partially responsible for the biological effects of PDNVs. For example, phosphatidic acid in PDNVs binds to HBP 35 proteins, which inhibits the growth of pathogens. Moreover, ceramide in some PDNVs affects the function of macrophages, which causes an effect on the tumor (31,32,33). In terms of protein, PDNVs have cytoplasmic proteins (actin, protease) and membrane proteins (aquaporin). Structural proteins such as tetraspanins are very important for maintaining the morphology and stability of the vesicle. On the other hand, there may also be proteins such as heat shock proteins that help package the cargo and form the vesicle. There are also proteins on the surface of the PDNVs membrane that mediate the interaction with target cells (33,34). In addition, PDNVs are enriched with different nucleic acid species that can regulate recipient cell genes, including miRNAs. Jiang et al. demonstrated, PDNVs' miRNAs may be considered a new class of micronutrients responsible for the medical properties of plants. Generally, plant miRNAs are involved in gene targeting, and the literature reports their beneficial role in some pathological conditions such as cancer. For example, plant miR-159 is correlated with a decrease in breast cancer incidence and progression. In particular, TCF7 is a mammalian target for plant miR-159, and it has shown the anti-proliferative function of miR-159 in breast cancer cells; demonstrating that a plant miRNA can influence cancer cell growth. Furthermore, a synthetic mimic of miR-159 can inhibit proliferation by targeting the TCF7 that encodes a Wnt signaling transcription factor, leading to a decrease in MYC protein levels (35).

Emerging studies have pointed out the role of miRNAs, packed in PDNVs, in the regulation of mammalian genes. Potestà et al. demonstrated that EVs derived from Moringa oleifera seeds, which carry plant miRNAs, can naturally penetrate inside human tumor cells and have proapoptotic effects. In particular, these EVs can modulate activities related to the viability and apoptosis in tumor cell lines, thanks to the regulation being mediated by miRNAs of BCL2 protein, which is one of the main factors that affects tumorigenesis in cell lines of epithelial origin (36).

1.3.3. Therapeutic Activities of PDNVs

One of the promising candidates for the treatment of several human diseases, including cancer, is PDNVs. In different studies, anti-proliferative and pro-apoptotic activities against cancer cells were observed by PDNVs derived from citrus fruits, ginger, bitter melon, and other sources (37). Lemon-derived PDNVs induce apoptosis via the TRAIL/Dr5 pathway in tumor cells, while bitter melon-derived PDNVs interact with chemotherapy to enhance treatment outcomes in oral squamous cell carcinoma by preventing drug resistance and promoting synergistic cytotoxic effects (38). In addition, grape-derived nanovesicles are being investigated in clinical trials for their potential to prevent oral mucositis associated with chemotherapy and radiation therapy in head and neck cancer patients (39). Another therapeutic aspect of PDNVs is their anti-inflammatory activities, which hold promise for the management of chronic inflammatory diseases such as inflammatory bowel disease (IBD). PDNVs derived from grapefruit have immunomodulatory effects and protect against colitis in animal models by modulating the expression of pro-inflammatory cytokines and promoting intestinal barrier function (40). In addition, PDNVs derived from other plant sources such as broccoli, carrot, and lemon have also shown anti-inflammatory effects, indicating the potential of PDNVs as natural anti-inflammatory agents (41,42). One of the main properties of PDNVs is their antioxidant properties, which reduce oxidative stress. As a result, they have a direct effect on cardiovascular diseases and neurological disorders. Studies have reported that PDNVs derived from different plant sources have antioxidant activities and protect cells from oxidative damage by scavenging reactive oxygen species (ROS) and increasing the expression of antioxidant genes (43). In this context, lemon-derived PDNVs have been evaluated for their antioxidant effects, confirming their ability to reduce ROS levels and neutrophil migration in LPS-stimulated zebrafish embryos (44).

Another property of PDNVs is regeneration, which facilitates wound healing and tissue repair. Studies in this field have shown that PDNVs derived from wheat and grapefruit promote skin

regeneration by inducing cell proliferation, migration, and angiogenesis in vitro. They also increase the expression of wound repair factors and collagen production, indicating their potential to accelerate wound closure and tissue regeneration (45,46). In addition, PDNVs derived from grapefruit have shown the ability to induce the proliferation of intestinal stem cells, which contributes to the regeneration of intestinal epithelial tissue and the reconstruction of intestinal architecture, which may be useful for the treatment of intestinal-related diseases such as colitis (45, 46).

1.4. Utilizing Extracellular Vesicles as vehicles of exogenous molecules

According to the progress of research in the field of EVs and the understanding of their structure and function, one of the things that has attracted the attention of researchers is drug delivery by EVs (47). Innovation in drug delivery methods in certain diseases, especially cancer, can create a revolution (48). The primary advantages of drug delivery systems lie in their ability to enhance treatment outcomes at targeted sites while minimizing adverse effects and drug toxicity (49). However, challenges exist, especially with compounds such as therapeutic RNA, which struggle to penetrate cells due to their anionic charge and sensitivity to RNases, necessitating the use of carriers (50). Among the systems used for drug delivery, liposomes are an example of this and facilitate the transfer of agents such as doxorubicin to cancer cells (47). Other delivery systems, including micelles, dendrimers, nanocapsules, and peptide-based nanoparticles, offer promising avenues for therapy (51). Despite the successful translation into clinical settings for some of these carriers (52), issues such as cytotoxicity and immunogenicity persist and drive the exploration of alternatives such as EVs. EVs offer distinct advantages over synthetic carriers, characterized by low toxicity, high biocompatibility, and reduced immunogenicity. As efficient transporters, they are capable of transporting proteins, nucleic acids, and other biomolecules to target cells (53-56). Although EVs have demonstrated their efficiency in delivering chemotherapy drugs, loading drugs and nucleic acids into electric vehicles remains a challenging effort. The ability of EVs to act as nanocarriers for drug delivery has been proven, and they have been effectively used to deliver chemotherapeutic drugs (57,58). However, drug and nucleic acid loading into EVs is still a challenging method.

1.5. Cargo Loading Strategies and therapeutic outcomes for Drug Delivery

Potential therapeutic cargoes, which include RNA, proteins, and drugs, can be loaded into PDNVs and mammalian EVs and different strategies can be followed for this purpose. It is known from experience with cell-derived exosomes, that it is possible to load exogenous

molecules by employing passive and active loading techniques. Some of the most widely used are co-incubation, sonication, electroporation, and transfection (Figure 5) (59,60).

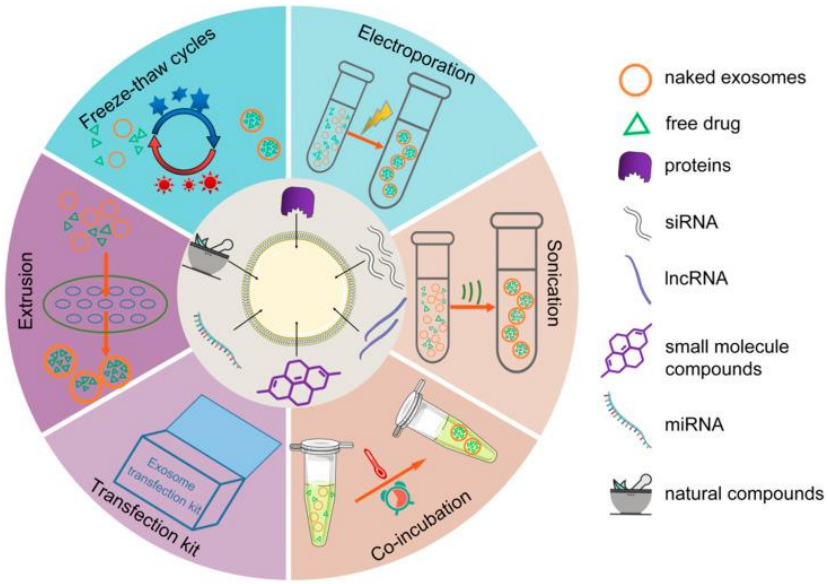

Figure 5. Post-secretory loading methods of EVs. Drug encapsulation strategies for isolated exosomes include sonication, electroporation, co-incubation, freeze-thaw cycles, extrusion, transfection kits (Sun K, et al. 2022).

Due to the lipidic nature of the PDNV membrane, various hydrophobic or amphiphilic drug compounds can be passively loaded into exosomes by co-incubation. According to this technique, Deng W et al loaded microRNA 34a into exosomes derived from the HEK 293 cell line. They showed that this complex prevents the proliferation, migration, and invasion of HN-6 cells (60). Also, Didiot MC et al. showed that the co-incubation of hsiRNAs with exosomes is an efficient method for loading exosomes with oligonucleotide cargo, and in this study, they investigated the delivery of this cargo in mouse brain neurons (61). In contrast, hydrophilic drugs and macromolecules require transient permeabilization of the vesicle membrane to be encapsulated. This is achieved by applying techniques such as electroporation or sonication (62). To date, electroporation has found extensive applications in the context of nanovesicles but has never been used in the field of PDNVs. The technique makes use of the administration of short high-voltage pulses that can induce a transient and reversible rupture of the membrane. It is possible to exploit this rupture to load the molecules of interest inside the vesicles (63). Although in most cases work using electroporation shows good loading efficiency (about 20–25% (64)), the technique has limitations: for example, one of the most common disadvantages is the aggregation or fusion of vesicles because of the electrical pulses (65). Like electroporation, another widely used technique for loading extracellular vesicles of various origins is sonication. In this case, the momentary membrane permeabilization occurs by ultrasonic waves that damage the integrity of the membrane and facilitate the capture of drugs or other substances of interest

(66). In this regard, Salarpour et al. produced a drug delivery system using the sonication method. In this study, they successfully loaded PTX in exosomes derived from the U87 cell line, and they also showed that PTX encapsulated in exosomes has a less toxic effect than free PTX (67). In the electroporation method, Van et al. investigated the siRNA loaded by electroporation in the exosome and the performance of CLTC against this complex. CLTCs play an important role in the uptake of exosomes by macrophages (68). As with mammalian-derived extracellular vesicles, it is very common to use transfection techniques for loading nucleic acids, including miRNAs into PDNVs. In the study conducted by Lorenadel Pozo-Acebo, the potential of carrying exogenous miRNA by broccoli vesicles was investigated (69). Nanovesicles were isolated from broccoli flower heads and then five groups of RNAs were extracted, such as ath-miR159a, ath-miR159b-3p, ath-miR166b-3p, ath-miR319a, and ath-miR403-3p mimics. To assess if broccoli isolated EVs could be loaded with exogenous miRNAs with potential therapeutic capacity, these were transfected with the five previously selected miRNA candidates. In this study, to understand the function of miRNA-loaded broccoli EVs, the complex was incubated with Caco-2 cells and the evidence showed that the cell viability decreased after the treatment. It was also found that EVs derived from broccoli can protect miRNA against RNase and gastrointestinal digestion (27,69). You et al. also used transfection agents to encapsulate miR-184 within cabbage exosome-like nanovesicles and were able to deliver it to colon cancer cells (70). In the same study, the research team also investigated the possibility of encapsulating doxorubicin in nanoparticles derived from cabbage by simple incubation. The vesicles containing doxorubicin effectively suppressed the proliferation of colon cancer cells and cell viability was dramatically reduced after treatment (27,70).

The exploration of EVs and PDNVs-mediated cargo transport has unveiled a complex and finely regulated communication network in both physiological and pathological conditions. Understanding these delivery mechanisms opens avenues for therapeutic applications, utilizing EVs and PDNVs as carriers for targeted drug delivery, diagnostics, and potential interventions in various diseases (42,45).

In our study, we aimed to develop and optimize methods for loading siRNAs and miRNAs into plant-derived nanovesicles and mammalian extracellular vesicles. We chose electroporation as the loading method due to its established efficacy in encapsulating RNA molecules. Our selection of specific RNA targets, including DDHD1 siRNA, miR-146a, and miR-199a, was based on previous observations and findings from our research group.

CHAPTER 2

Objectives

As elucidates in introduction, a multitude of methodologies have been employed to encapsulate diverse pharmaceutical compounds within EVs. Most of the data are focused on animal-derived EVs; however, in recent years, numerous studies have been carried out on PDNVs. PDNVs can be purified from different parts of the plant, such as roots, leaves, fruits, and seeds (33,75), and participate in intercellular interactions also across different kingdoms (76,77). We demonstrated that NVs isolated from lemon juice have anti-cancer effects by activating apoptosis (33). Another study conducted in 2018 showed that NVs extracted from ginger can be used to transfer therapeutic siRNAs to tumor cells and inhibit tumor growth (78). However, very few studies about siRNAs loading strategies into plant NVs are currently available. The aims of this study are to isolate and characterize extracellular vesicles (EVs) derived from tangerine juice (TNVs) and to develop an efficient protocol for loading these TNVs with exogenous small interfering RNAs (siRNAs) specifically targeting DDHD1. DDHD1 is a gene whose overexpression has been linked to an increased proliferation rate in colon cancer cells. By targeting DDHD1 with siRNAs, we aim to suppress its expression and consequently inhibit the proliferation of colon cancer cells. This research seeks to explore the potential of TNVs as a novel delivery system for siRNA-based therapies, providing a foundation for further development of non-toxic, natural delivery vehicles in cancer treatment. (79).

CHAPTER 3

Materials and Methods

3.1. Tangerine Nanovesicles Isolation

TNVs have been isolated by differential centrifugation, filtration, and ultra-centrifugation from tangerine juice (Citrus reticulata Blanco), obtained from the company Agrumaria Corleone s.p.a. (Palermo, Italy). Given the citrus fruit's seasonality, the annually produced fresh juice was frozen at -20°C to have the possibility to work over the year; indeed, the experiments reported in this study were carried out using the juice produced in the same year. After thawing at 4°C, the juice was centrifuged at 3,000 × g for 15 min, and 10,000 × g for 30 min. The supernatant was filtered at 0.8 μm and centrifuged at 16,500 × g for 1 h, then the obtained supernatant was filtered at 0.45 μm pore filter and centrifuged at 16,500 × g for 2 h. The resulting supernatant was then ultra-centrifuged at 100,000 × g for 1 h and 45 min in a Type 70 Ti, fixed angle rotor. The pellet, containing the vesicles was washed and suspended in phosphate-buffered saline (PBS). TNV protein quantification was determined with the Bradford assay (Pierce, Rockford, IL, USA). On average, we recovered 120-180 micrograms of vesicles from 240 ml of tangerine juice (Figure 6).

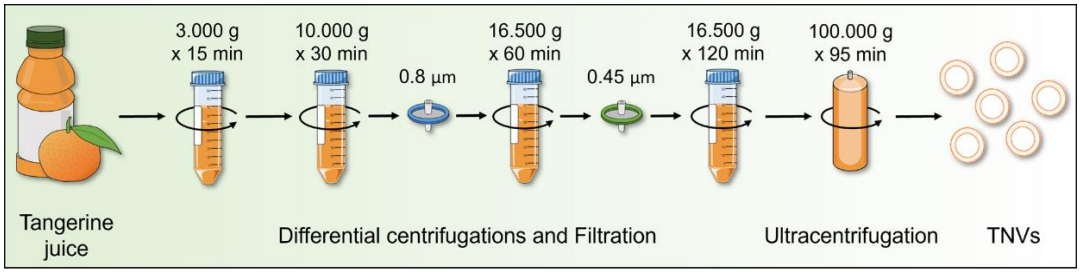

Figure 6. Schematic illustration of the protocol of TNV isolation.

3.2. Nanoparticle Tracking Analysis

Concentrations and size distribution of tangerine vesicles were measured by Nanoparticle Tracking Analysis (NTA) (NanoSight NS300, Malvern Instruments Ldt, UK). TNV samples were diluted 1:100 in PBS to reach optimal concentration for instrument linearity. The particle

size measurement was calculated on a particle-by-particle basis in 3 videos of 60 s to provide accuracy and statistics for each analysis, under the following conditions: cell temperature: 23.3°-23.6°C; Syringe speed: 30 µl/s. Recorded data were analyzed for the mean, mode, median, and estimated concentration of particles by the in-build NanoSight Software NTA 3.3 with a detection threshold of 5. Hardware: embedded laser: 45 mW at 488 nm; camera: sCMOS.

3.3. Dynamic Light Scattering

Exosome size distribution was determined by Dynamic Light Scattering (DLS) experiments. Collected nanovesicle samples were diluted in Milli-Q water (2 times for untreated vesicles, 20 times for electroporated ones) and centrifuged at 1,000 × g for 10 min at 4 °C. The supernatant was placed at 20 °C in a thermostated cell compartment of a Brookhaven Instruments BI200-SM goniometer, equipped with a He-Ne laser (JDS Uniphase 1136P) tuned at 633 nm and a single-pixel photon counting module (Hamamatsu C11202-050). Scattered light intensity and its autocorrelation function $g_2(t)$ were measured simultaneously at a scattering angle of 90° by using a Brookhaven BI-9000 correlator. The intensity autocorrelation function $g_2(t)$ is related to the size σ of diffusing particles and to their (z-averaged) size distribution $P_q(\sigma)$, by the relation $g2(t) = 1 + |\beta \int P_q(\sigma) \exp[-D(\sigma)q^2t]|^2$, where β is an instrumental parameter, $q = 4\pi \tilde{n} \lambda^{-1} \sin[\vartheta/2]$ is the scattering vector, with ñ being the refractive index of the medium, and D(σ) is the diffusion coefficient of a particle of hydrodynamic diameter σ, determined by the Stokes-Einstein relation $D(\sigma) = k_B T[3\pi\eta\sigma]^{-1}$, with T being the temperature, η the medium viscosity, and kB the Boltzmann constant (80). The size distribution $P_q(\sigma)$ is calculated by assuming that the diffusion coefficient distribution is shaped as a Schultz distribution, which is a two-parameter asymmetric distribution, determined by the average diffusion coefficient $\underline{D}$ and the polydispersity index PDI (81,82).

3.4. Cell Culture

The human colorectal adenocarcinoma cell line, SW480, was obtained from ATCC (Manassas, VA, USA) and was cultured in RPMI 1640 medium (Euroclone, UK) supplemented with 10% fetal bovine serum (FBS, Euroclone), 2 mM L-glutamine (Euroclone), 100 U/ml penicillin and 100 µg/ml streptomycin (Euroclone).

Human dermal fibroblasts (HDFα) were obtained from ATCC (Manassas, VA, USA) and were cultured in Fibroblast Basal media (ATCC, Manassas, VA, USA) supplemented with Fibroblast Growth Kit-Low serum (ATCC, Manassas, VA, USA), 100 U/ml penicillin, and 100 µg/ml streptomycin (Euroclone, UK).

Human stromal cells (HS5) were grown in high glucose DMEM medium supplemented with 10% fetal bovine serum, 100 U/mL penicillin, and 100 µg/ml streptomycin (Euroclone, UK). Caco-2 cell line (ATCC, Manassas, VA, USA) was cultured in Eagle's Minimum Essential Medium supplemented with 20% FBS.

SV40 large T antigen-immortalized normal human liver epithelial cell line, THLE2 (ATCC, Manassas, VA), was cultured in LHC-8 Basal Medium (Invitrogen, Carlsbad, CA) supplemented with 70 ng/ml phosphoethanolamine, 5 ng/ml epidermal growth factor (EGF), 10% fetal bovine serum, 100 U/mL penicillin, and 100 µg/ml streptomycin (Euroclone, UK). Cells were maintained in precoated flasks with a collagen coating made of a mixture of 0.03 mg/ml bovine collagen type I (Advanced Biomatrix, San Diego region, California, USA) and 0.01 mg/ml bovine serum albumin (Sigma-Aldrich, St Louis, MO, USA).

SW480, HDFα, HS5, Caco-2 and THLE2 cells were grown in a 37 °C humidified incubator with 5% CO2 and were passaged every 2-3 days.

3.5. Western Blotting

The protein lysates from TNVs and SW480 cells treated for 48 h with TNVs (25 µg/ml) or TNVs (25 µg/ml) loaded with 200 pmol of scrambled siRNA or DDHD1-siRNA were analyzed by SDS-PAGE followed by Western blotting. The antibodies used in the experiments were anti-HSP70 (Agrisera, Vännäs, Sweden), anti-DDHD1 (Novus Biologicals, Bio-Techne SRL Milan, Italy), and anti-GAPDH (Santa Cruz Biotechnology). Membranes were incubated with HRP-conjugated secondary antibody (Thermo Fisher Scientific, Cambridge, MA, USA) and the chemiluminescent signal was detected with Chemidoc (Biorad, Milan, Italy).

3.6. Transmission Electron Microscopy

The isolated TNVs resuspended in PBS were identified by transmission electron microscopy studies using negative staining. A 10 µl aliquot of TNVs suspension was dropped onto 200 mesh carboncoated EM grids, followed by standing at ambient temperature for 10 min. After washing with ddH_2O, the samples were fixed for 5 min in 1% glutaraldehyde. Subsequently, the TNVs were negatively stained with a 2% aqueous solution of phosphotungstic acid. After air drying, the grids were visualized in a JEM 1400 Plus electron microscope (Jeol, Japan) operating at 80 kV.

3.7. Zeta Potential

The Zeta potential of TNVs was measured using a Zetasizer nano ZSP (Malvern, UK). The TNVs (6 µg) were diluted in a solution containing 1 mM NaCl to a total volume of 0.6 mL; the pH of the solution was 7.8. The sample was transferred to the specific cuvette for zeta potential measurement (disposable capillary cell, DTS1070, Malvern, UK).

3.8. Atomic Force Microscopy

Sample preparation: glass slides were functionalized according to the following treatment: (i) cleaned by immersion in boiling acetone for a few minutes, dried in a stream of high-purity nitrogen, and exposed to UV rays (30W Hg lamp) for 1 h to expose the hydroxyl groups of silica; (ii) treated with a 0.25 M (3-aminopropyl)-triethoxysilane (APTES) in chloroform solution for 5 min at room temperature, and then rinsed with chloroform and dried with nitrogen; (iii) treated with 0.4 M glutaraldehyde aqueous solution for 5 min at room temperature and then rinsed with Milli-Q water and dried with nitrogen. 30 µl of vesicle solution (diluted 200 times in PBS after centrifugation at 1,000 × g for 10 min at 4 °C) was deposited onto functionalized glass slides and incubated overnight. Vesicle imaging: samples were gently rinsed by PBS and Quantitative Imaging AFM measurements were carried out in PBS by using a Nanowizard III scanning probe microscope (JPK Instruments AG, Germany) equipped with a 15 µm z-range scanner, and AC40 (Bruker) silicon cantilevers (spring constant 0.1 N/m, typical tip radius 8 nm). 5 x 5 μm^2 images were acquired at 512x512 pixels resolution and force setpoint 150 pN (z-length: 50 nm and 70 nm, pixel time: 5 ms and 7 ms for untreated and electroporated samples respectively). In the electroporated sample, we set a higher z-length in response to the observed higher adhesion, which is likely caused by spurious sticky molecules or fragments due to electroporation. The cantilever was thermally calibrated by using the tool in JPK software (83). Statistical analysis: it was performed using the grain analysis tools, available on Gwyddion software ver 2.62. In particular, the equivalent discradius of the objects was computed, and the grains ascribed to nanovesicles were selected by the following criteria: a) height greater than 10 nm (limit case for two overlapped lipid bilayers) and b) area greater than 15 pixels (to skip eventual spikes and objects that are too small to be recognized as nanovesicles).

3.9. Proteomics

3.9.1. Sample Preparation

About 10 µg of TNV protein lysate was subjected to proteolytic digestion using filter-assisted sample preparation (FASP) protocol with 10 kDa Vivacon spin filters (Sartorius, Göttingen, Ger-

many). Briefly, proteins were reduced by the addition of 1 M Dithiothreitol (DTT, Thermo Fischer Scientific) in 100 mM Tris/HCl, 8 M urea pH 8.5 for 30 min at 37 °C. Proteins were then alkylated in 50 mM iodoacetamide (IAA, Thermo Fischer Scientific) for 5 min at room temperature and washed twice in 100 mM Tris/HCl, 8 M urea pH 8.0 at 14,000× g for 30 min. Proteins were digested with 0,2 µg LysC (Promega, Madison, United States) in 25 mM Tris/HCl, 2 M urea pH 8.0 overnight and with 0,1 µg trypsin (Promega) in 50 mM ammonium bicarbonate for 4 h. Resulting peptides were desalted by stop-and-go extraction (STAGE) on reverse phase C18 (Supelco Analytical Products, part of Sigma-Aldrich, Bellefonte, US), and eluted in 40 µL of 60% acetonitrile in 0.1% formic acid. Then, volume was reduced in a SpeedVac (Thermo Fisher Scientific) and the peptides resuspended in 20 µL of 0.1% formic acid. Peptide concentration was measured by a NanoDrop microvolume spectrophotometer (Thermo Fischer Scientific) and 1 µg peptides were applied to LC-MS/MS analysis.

3.9.2. LC-MS/MS

To achieve high sensitivity, a nanoLC system (Vanquish Neo UHPLC – part of Thermo Scientific) using an Acclaim PEPMap C18 column (25cm × 75 µm ID, Thermo Scientific, Waltham) was coupled online to an Exploris 480 mass spectrometer (Thermo Fischer Scientific). Peptides were separated using a 130 minutes binary gradient of water and acetonitrile containing 0.1% formic acid. Data-independent acquisition (DIA) was performed using a MS1 full scan (400m/z to 1200m/z) followed by 60 sequential DIA windows with an overlap of 1m/z and window placement optimization option enabled. Full scans were acquired with 120000 resolution, automatic gain control (AGC) of 3x106, and maximum injection time of 50ms. Afterwards, 60 isolation windows were scanned with a resolution of 30000, an AGC of 8x105 and maximum injection time was set as auto to achieve the optimal cycle time. Collision induced dissociation fragmentation was induced with 30% of the normalized HCD collision energy.

The data were analysed by the software DIA-NN (version 1.8.1) by using a predicted library generated from in silico digested Citrus sinensis (UP000027120) Uniprot reference database involving cuts at K* and R*, two missed cleavage allowed, minimal peptide length set at 6. The false discovery rate for peptide and protein identification was set at 0.01%.

3.10. Reversed-Phase HPLC/MS

The water and acetonitrile were of HPLC/MS grade. Formic acid was of analytical quality. The analyses were performed by adapting a previously reported method (55). The HPLC system was an Agilent 1260 Infinity. A reversed-phase Agilent Poroshell 120 EC-C18 column

(50mm×3.0mm, particle size 2.7µm) with a Phenomenex C18 security guard column (4mm×3mm) was used. The flow rate was 0.4 mL/min, and the column temperature was set to 30 °C. The eluents were formic acid–water (0.1:99.9, v/v) (phase A) and formic acid–acetonitrile (0.1:99.9, v/v) (phase B). The following gradient was employed: 0–10 min, linear gradient from 5% to 95% B; 10–12 min, reconditioning to 5% B; 12–15 min, 5% B isocratic. The injection volume was 15 µL. The eluate was monitored through MS TIC. Mass spectra were obtained on an Agilent 6540 UHD accurate-mass Q-TOF spectrometer equipped with a Dual AJS ESI source working in negative mode. N2 was employed as desolvation gas at 320 °C and a flow rate of 7 L/min. The nebulizer was set to 20 psig, the Sheat gas temperature was set at 295 °C, and a flow of 8 L/min. A potential of 2.6 kV was used on the capillary for negative ion mode. The fragmentor was set to 175 V. MS spectra were recorded in the 100–3200 m/z range. TNVs samples for HPLC were analyzed "as is". Reproducibility was verified with 3 replicates. Mass spectrum data were analysed for metabolites annotation using MassHunter Qualitative Analysis B.06.00 and the Metlin database [METLIN. Available online: https://metlin.scripps.edu/landing_page.php?pgcontent=mainPage].

3.11. Cell Viability Assays

Cell viability was assessed with the MTT assay (3-[4,5-Dimethylthiazol-2-yl]-2,5 Diphenyl Tetrazolium Bromide). Different cell lines, HDFα, HS5, THLE2, SW480 and Caco-2 cells, were seeded in triplicate in 96-well plates at a density of 10,000 cells/well and treated after 24 h with different doses of TNVs (1; 5; 10; 25 µg/ml). Viability was evaluated at 24 and 48 h. Cells were also treated with 10% DMSO as positive control of cell death. In addition, to determine the effects of siRNA loaded TNVs on the viability of colorectal cancer cells, SW480 cell lines were seeded at 10,000 cells/well in duplicate in 96-well plates. 24 h after seeding, cells were treated with 25 µg/ml of TNVs previously loaded with 200 and 400 pmol of scrambled or DDHD1-siRNA. Cell viability was measured after 48 h. For all cell lines above mentioned, the absorbance was measured by an ELISA reader at 540 nm (Microplate Reader, BioTek, Winooski, VT, USA). Values are expressed as a percentage of cell growth versus control (untreated cells).

3.12. TNV Internalization in Human Cell Lines

TNVs were incubated with PKH26 Red Fluorescent Cell Linker Kits (Merck KGaA, Darmstadt, Germany) for 15 minutes, washed three times with PBS and then resuspended in cell culture medium. Labelled TNVs were incubated for 2 hours with SW480, and Caco-2 cell lines at 37°C. Following treatment, to verify the TNV internalization, cells were fixed with PFA 4% and

permeabilized with TritonX-100. Cellular actin was stained with Actin Green (Molecular Probes, Life Technologies, Carlsbad, CA, USA), while Nuclei with Hoechst (Molecular Probes, Life Technologies, Carlsbad, CA, USA). The samples were analysed by confocal microscopy (Nikon A1, Amsterdam, Netherlands). Data are expressed as the mean fluorescence intensity calculated on cell surface.

3.13. siRNA Labeling

To evaluate the loading of siRNA inside the TNVs, labeling of scrambled and DDHD1-siRNA with Cy3 was performed using the Silencer siRNA labeling kit (Thermo Fisher Scientific). We prepared 5 pmol of Cy3-scrambled and Cy3-DDHD1-siRNA by following the manufacturer's protocol. Briefly, Cy3 powder was dissolved with the reconstitution solution provided by the kit and incubated at 25 °C for 5 min. Then, a mixture containing siRNA, Cy3, labeling buffer, and H2O was prepared. The Cy3-siRNA mix was incubated, protected from light, at 37 °C for 1 h, then 100% cold ethanol and 5 M NaCl were added; the mix was vortexed, kept at -20 °C for 1h, and centrifuged for 20 min at 10,000 g. The supernatant was removed while the pellet was washed in 70% ethanol; the mix was centrifuged for 10 min at 10,000 g. Finally, the supernatant was removed, and the pellet air dried at room temperature for 15 min and then suspended in nuclease-free H2O. The fluorescence was measured with GloMax®-Multi Detection System Protocol (Promega) to verify the labeling.

3.14. TNVs Electroporation

Electroporation was performed in a 0.2 cm–gap sterile electroporation cuvette. TNVs (25 µg) were mixed with Cy3-scrambled-siRNA or Cy3-DDHD1-siRNA (20; 50; 100; 200 pmol) and suspended in electroporation buffer (1.15 mM potassium phosphate, 25 mM potassium chloride, and 21% OptiPrep in PBS). The samples were electroporated at 2,000 V for 0.8 ms and then incubated at 37 °C for 1 h to allow recovery of the nanovesicle membrane. Then the sample was centrifuged at 14,000 x g for 20 min to remove the not-loaded siRNA (Figure 7). The supernatant was collected, while the pellets containing electroporated TNVs were resuspended in PBS and used for cell treatment. Finally, the fluorescence of the complex Cy3-siRNA-TNVs and the supernatant were quantified at GloMax®-Multi Detection System.

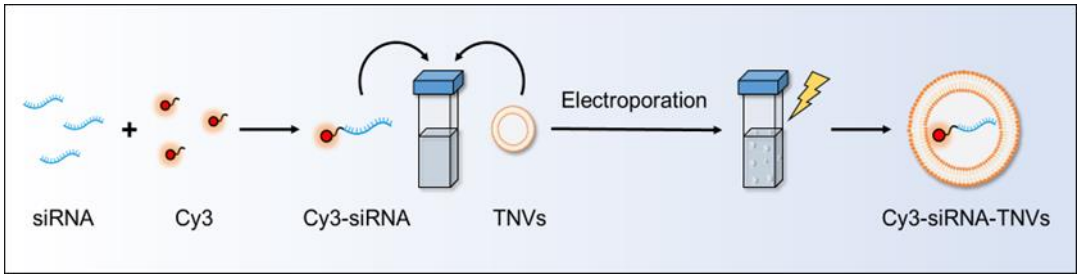

Figure 7. Cy3-siRNAs loading in TNVs through electroporation. (A) Schematic illustration of the protocol of TNV electroporation.

3.15. RNAse Treatment

Electroporated TNVs were treated with 10 µg/mL of Ribonuclease A (RNAse A) and incubated at 37 °C for 30 min. The sample was centrifuged at 14,000 x g for 20 min; the supernatant was removed, while the pellets were washed and resuspended in PBS. The fluorescence of the complex TNVs-Cy3-siRNA was quantified at GloMax®-Multi Detection System.

3.16. Confocal Microscopy

SW480 cells were seeded at 100,000 cells/well (8 well chambers) and, after 24 h, treated with Cy3-DDHD1-siRNA TNVs (25 µg of TNVs loaded with 200 pmol of scrambled siRNA) for 24 h. At the end of the experiment, the cells were fixed with PFA 4%, permeabilized with 0.1% TritonX-100, and stained with Actin Green (Molecular Probes, Life Technologies, Carlsbad, CA, USA) and Hoechst (Molecular Probes, Life Technologies, Carlsbad, CA, USA). The samples were analyzed by confocal microscopy (Nikon A1, Amsterdam, Netherlands).

3.17. Cell Transfection

Transfection of DDHD1-siRNA in SW480 was performed using the HiPerFect Transfection Reagent (Qiagen) according to the manufacturer's instructions. Cells were plated in 24-well plates and 24 h after seeding were transfected with 200 pmoles/mL of DDHD1-siRNA. 48 h after transfection the cells were processed for RNA isolation and Real-Time PCR.

3.18. RNA Isolation and Real-Time PCR

SW480 cells were seeded in 12-well plates at 300,000 cells/well. After 24 h, the cells were treated with scrambled-siRNA TNVs and DDHD1-siRNA TNVs (25 µg of TNVs loaded with 200 pmol of scrambled or DDHD1-siRNA) and with respective supernatants collected after TNVs electroporation for 24 and 48 h. At the end of the treatments, total RNA was extracted using Illustra^{TM} RNA spin mini-RNA isolation Kit according to the manufacturer's instructions (GE Healthcare, Little Chalfont, Buckinghamshire, UK). The RNA was reverse transcribed to cDNA

using the High-Capacity cDNA Reverse Transcription kit (Applied Biosystems, Foster City, CA, USA). Then, RT-QPCR was performed in 48-well plates using Step OneTM Real-time PCR System Thermal Cycling Block (Applied Biosystem).

Gene	Forward 5'→3'	Reverse 5'→3'
ACT	TCCCTTGCCATCCTAAAAAGCCACCC	CTGGGCCATTCTTCCTTAGAGAGAAG
DDHD1	TTTCTCAACCCAGCTAAAGAACCTA	TGATCCAACTCCAATGCAGAAT

Table 1. The sequences of the primers used for quantitative SYBR®Green real-time PCR

Target transcript levels were normalized against the endogenous control GAPDH, consistently expressed in all samples (ΔCt). For each condition, final values were expressed as the DDHD1 level normalized to the endogenous control ($2^{\wedge-\Delta CT}$).

3.19. Statistical Analysis

Data are expressed as mean ± SD of biological replicates. Statistical analysis was performed using GraphPad Prism software (GraphPad Software, Inc, La Jolla, CA). The normal data distribution was assessed by Shapiro-Wilk test. When data follow normal distribution, the statistical significance of the differences was analysed using a two-tailed Student's t-test; otherwise, non-parametric method (Mann-Whitney test) were used to compare the groups. A p-value ≤ 0.05 was considered significant.

CHAPTER 4

Results

4.1. Isolation and Characterization of Tangerine-Derived Nanovesicles (TNVs)

As shown in Figure 6 in the method section, TNVs were isolated from the fruit juice using the differential centrifugation method. Once isolated, TNVs were characterized through Nanoparticle tracking analysis (NTA), western blot, transmission electron microscope (TEM), and atomic force microscope (AFM). NTA analysis showed that TNVs had a heterogeneous size distribution, with a mean of 255 nm ± 18 nm and a mode of 180 nm ± 14 nm (Figure 8A). DLS analysis confirmed these results showing a size distribution with a z-average size of 236 ± 3 nm, a mode of 187 ± 3 nm, and a polydispersity index of 0.26 (Figure 8B).

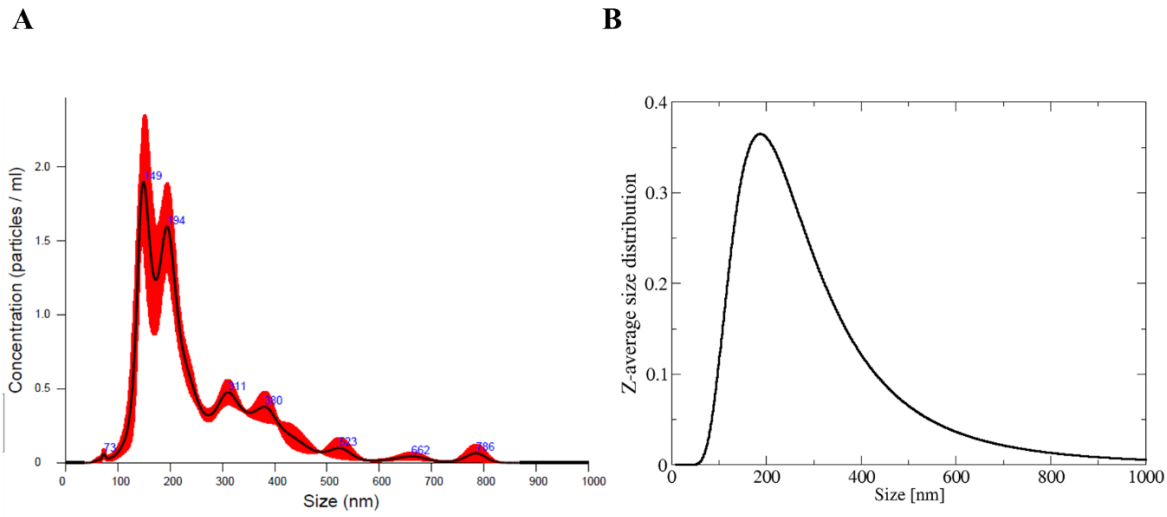

Figure 8. (A) Size distribution of TNVs obtained through NTA. (B) Size distribution of TNVs obtained through DLS.

To gain more insight into the composition of plant nanovesicles and to search for relevant markers, we performed a proteomic analysis (minimal peptide length set at 6 and false discovery

rate set at 0.01%) on TNVs. In our investigation, we identified a repertoire of crucial biomolecules involved in the biogenesis and cargo sorting of nanovesicles. Specifically, our analysis revealed the presence of heat shock proteins HSP70 and HSP90, which are known for their roles in mediating cellular stress responses and facilitating the folding and transport of proteins (84). Furthermore, our findings indicate the presence of tetraspanins, a family of transmembrane proteins recognized for their involvement in EV biogenesis, cargo packaging, and intercellular communication (85). Additionally, annexins, known for their membrane-binding properties and implication in vesicle formation and trafficking, were also identified within the EV cargo repertoire (86). Moreover, our investigation unveiled the presence of ATP-binding cassette (ABC) transporters, which are integral membrane proteins implicated in the selective packaging of cargo molecules into EVs and are crucial for EV-mediated intercellular communication (87). Lastly, our analysis revealed the presence of glyceraldehyde-3-phosphate dehydrogenase (GAPDH), a ubiquitous metabolic enzyme, which has been implicated in EV biology, suggesting its potential role in vesicular cargo sorting or metabolic regulation within recipient cells (88). These findings collectively contribute to our understanding of the molecular constituents and functional properties of EV cargo, shedding light on the intricate mechanisms underlying EV biogenesis and intercellular communication. (Table 2). These proteins belong to different families identified in mammalian vesicles (10) and in plants, as also re-viewed in a letter to the editor by Pinedo and colleagues in 2021 (26).

AC Number *	**Entry Name ***	**Gene Name**	**Protein Description**
A0A067EJK1	A0A067EJK1_CITSI	CISIN_1g043296mg	Heat shock protein 70
A0A067DI64	A0A067DI64_CITSI	CISIN_1g006381mg	Heat shock protein 70
A0A067DCX3	A0A067FND2_CITSI	CISIN_1g0092461mg	Heat shock protein 70 (Fragment)
A0A067FZV6	A0A067FZV6_CITSI	CISIN_1g036208mg	Heat shock protein 70 (Fragment)
A0A067GGS2	A0A067GGS2_CITSI	CISIN_1g008233mg	Heat shock 70 kDa protein 8
A0A067FAC8	A0A067FAC8_CITSI	CISIN_1g002363mg	Heat shock 70 kDa protein 17
A0A067DSB8	A0A067DSB8_CITSI	CISIN_1g047555mg	Chloroplast heat shock protein 70 (Fragment)
A0A067FSA0	A0A067FSA0_CITSI	CISIN_1g0038272mg	Heat shock protein 90 (Fragment)
A0A067F0T0	A0A067F0T0_CITSI	CISIN_1g005370mg	Histidine kinase/HSP90-like ATPase domain-containing protein
A0A067F4L3	A0A067F4L3_CITSI	CISIN_1g003713mg	Histidine kinase/HSP90-like ATPase domain-containing protein
A0A067FVU3	A0A067FVU3_CITSI	CISIN_1g0038271mg	Histidine kinase/HSP90-like ATPase domain-containing protein (Fragment)

A0A067G9H4	A0A067G9H4_CITSI	CISIN_1g005321mg	Histidine kinase/HSP90-like ATPase domain-containing protein
A0A067GZ61	A0A067GZ61_CITSI	CISIN_1g003458mg	Histidine kinase/HSP90-like ATPase domain-containing protein
A0A067G5N9	A0A067G5N9_CITSI	CISIN_1g018146mg	Activator of Hsp90 ATPase AHSA1-like N-terminal domain-containing protein
A0A067H629	A0A067H629_CITSI	CISIN_1g034185mg	Heat shock factor binding protein
H9NHJ9	H9NHJ9_CITSI	hsp90	Hsp90
A0A067E0C1	A0A067E0C1_CITSI	CISIN_1g020485mg	ABC transporter domain-containing protein
A0A067ET19	A0A067ET19_CITSI	CISIN_1g000512mg	ABC transporter domain-containing protein
A0A067EWG6	A0A067F4Y3_CITSI	CISIN_1g000529mg	ABC transporter domain-containing protein
A0A067F105	A0A067F105_CITSI	CISIN_1g0005062mg	ABC transporter domain-containing protein (Fragment)
A0A067F137	A0A067F137_CITSI	CISIN_1g000615mg	ABC transporter domain-containing protein
A0A067F143	A0A067F143_CITSI	CISIN_1g037155mg	ABC transporter domain-containing protein (Fragment)
A0A067F413	A0A067F413_CITSI	CISIN_1g048654mg	ABC transporter domain-containing protein
A0A067F4N5	A0A067F4N5_CITSI	CISIN_1g0005061mg	ABC transporter domain-containing protein (Fragment)
A0A067F4X0	A0A067F4X0_CITSI	CISIN_1g0008381mg	ABC transporter domain-containing protein (Fragment)
A0A067GMU5	A0A067GMU5_CITSI	CISIN_1g024529mg	ABC transporter domain-containing protein
A0A067FAW9	A0A067FAW9_CITSI	CISIN_1g000702mg	ABC-type xenobiotic transporter
A0A067FGQ4	A0A067FGQ4_CITSI	CISIN_1g000481mg	ABC-type xenobiotic transporter
A0A067H5I7	A0A067H5I7_CITSI	CISIN_1g000438mg	ABC-type xenobiotic transporter
A0A067G6T3	A0A067G6T3_CITSI	CISIN_1g0003511mg	ABC-type xenobiotic transporter (Fragment)
A0A067GAY6	A0A067GAY6_CITSI	CISIN_1g000856mg	ABC transporter B family member 19
A0A067FNQ5	A0A067FNQ5_CITSI	CISIN_1g000750mg	ABC transporter B family member 20
A0A067FQJ3	A0A067FQJ3_CITSI	CISIN_1g006489mg	ABC transporter B family member 25
A0A067FY53	A0A067FY53_CITSI	CISIN_1g040300mg	ABC transporter E family member 2
A0A067FUW5	A0A067FUW5_CITSI	CISIN_1g002031mg	ABC1 atypical kinase-like domain-containing protein

A0A067FVU0	A0A067FVU0_CITSI	CISIN_1g009334mg	ABC1 atypical kinase-like domain-containing protein
A0A067G3Z9	A0A067G3Z9_CITSI	CISIN_1g023208mg	Tetraspanin-3-like
A0A067F4S7	A0A067F4S7_CITSI	CISIN_1g024170mg	Tetraspanin-8-like
A0A067FQS3	A0A067FQS3_CITSI	CISIN_1g022738mg	Tetraspanin-18-like
A0A067F2J1	A0A067F2J1_CITSI	CISIN_1g014424mg	Glyceraldehyde-3-phosphate dehydrogenase
A0A067H382	A0A067H382_CITSI	CISIN_1g019445mg	Glyceraldehyde-3-phosphate dehydrogenase
A0A067GQH6	A0A067GQH6_CITSI	CISIN_1g035973mg	Annexin
A0A067ERS2	A0A067ERS2_CITSI	CISIN_1g021204mg	Annexin

Table 2. Protein identified in TNVs. Heat Shock Proteins HSP70 and HSP90, Tetraspanins, Annexins, ABC transporters and the Glyceraldehyde-3-phosphate dehydrogenase.

Through Western blot, the presence of HSP70, a protein described as a marker of both animal and PDNVs (89) was confirmed (Figure 9A). Transmission electron microscope analysis showed that, after negative staining, the vesicles presented the morphological typical cup- or nearly round shapes (Figure 9B). The sizes were seen within the ranges between 40 and 150 nm which was consistent with the characteristics of small vesicles (10).

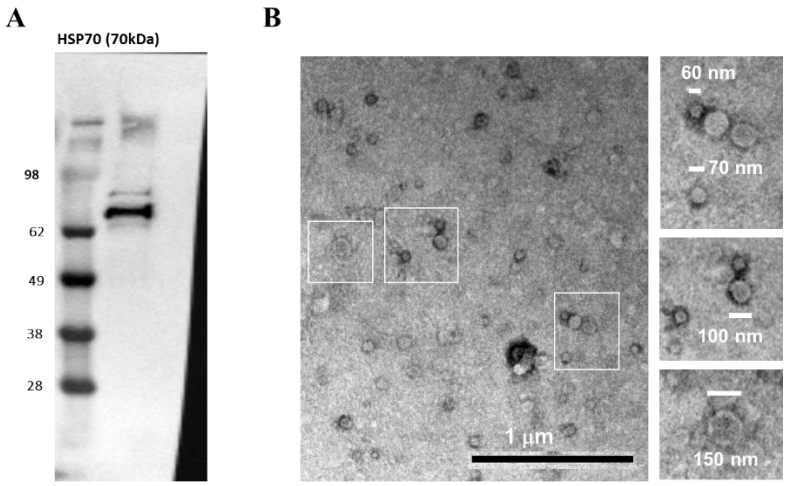

Figure 9. (A) Western blot analysis of HSP70 in TNVs. (B) Representative image and relative magnifications of transmission electron microscopic analysis showing the heterogeneity in size of the isolated TNVs.

In line with nanovesicles from other plant-species, TNVs have a negative Z-potential of -5.94 mV (Figure 10A). The AFM analysis showed that the apparent width of the TNV population ranges between 40 and 110 nm (Figure 10B). Since AFM sampling depends upon the particle number concentration, the size distribution measured by AFM indicates lower values with respect to the one measured by DLS and NTA, which are affected by the contributions of larger particles.

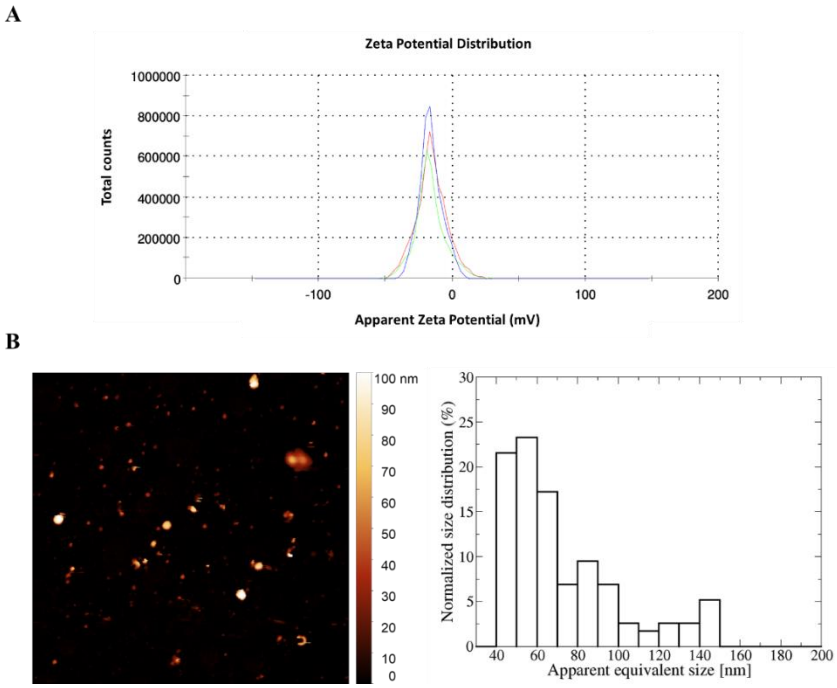

Figure 10. (A) Zeta potential of TNVs; the Zeta value (mV) is the meaning of three records. (B) Representative AFM image (5 x 5 µm2) of TNVs (left panel) and the related statistical analysis (right panel).

Furthermore, we performed a metabolomics analysis of TNVs and identified 35 compounds, summarized in Table 3. Detected compounds can be classified in different families such as organic acids, flavonoids, limonoids, Cinnamic acid derivatives, lysophospholipids, carbohydrates, and a salicylic acid derivative. All compounds are also present in the tangerine juice, but interestingly some of them were concentrated into nanovesicles (Figure 11). Tengeretin, quinic acid, diosmetindiglucoside, and lysophospholipids (except lysoPC(16:0)) were substantially concentrated in TNVs. Organic acids are unchanged, while limonoids and other flavonoids present lower concentrations in TNVs compared to juice.

	Compound	**Molecular formula**	**Chemical class**	**ESI$^-$[M-H]$^-$(m/z) (Teor.)**	**ESI$^-$[M-H]$^-$(m/z) (Exp.)**	**Rt (min)**
1	Arabinoside	$C_{10}H_{15}N_5O_5$	Carbohydrate	284.10	284.0970	3.33
2	Glutamic acid	$C_5H_9NO_4$	Aminoacid	146.0459	146.0459	3.42
3	Fructose	$C_6H_{12}O_6$	Carbohydrate	179.0561	179.0575	3.45
4	Quinic acid	$C_7H_{12}O_6$	Organic acid	191.0561	191.0551	3.77
5	Tangeretin	$C_{20}H_{20}O_7$	Methoxylated flavonoid	371.1136	371.1153	3.89
6	Methylisocitric acid	$C_7H_{10}O_7$	Organic acid	205.0354	205.0343	4.08
7	Ascorbic acid	$C_6H_8O_6$	Organic acid	175.0248	175.0246	4.19

8	Malic acid	$C_4H_6O_5$	Organic acid	133.0142	133.0143	4.29
9	Isocitric Acid	$C_6H_8O_7$	Organic acid	191.0197	191.0198	5.02
10	Citric Acid	$C_6H_8O_7$	Organic acid	191.0197	191.0192	5.26
11	Hesperetin	$C_{16}H_{14}O_6$	Methoxylated flavanone	301.0714	301.0671	6.58
12	Dehydroascorbic acid	$C_6H_6O_6$	Organic acid	173.0092	173.0086	7.10
13	Rutin	$C_{27}H_{30}O_{16}$	Non-methoxylated flavonol glycoside	609.1461	609.1404	7.57
14	Kaempferol-3-O-rutinoside	$C_{27}H_{30}O_{15}$	Non-methoxylated flavonol glycoside	593.1512	593.1461	7.67
15	Diosmetin diglucoside	$C_{28}H_{32}O_{16}$	Methoxylated flavone glycoside	623.1618	623.1580	7.74
16	Caffeic acid 3-O-glucuronide	$C_{15}H_{16}O_{10}$	Cinnamic acid derivative	355.0671	355.0645	7.95
17	O-Feruloylgalactarate	$C_{16}H_{18}O_{11}$	Cinnamic acid derivative	385.0776	385.0752	8.00
18	Salicylacyl glucuronide	$C_{13}H_{14}O_9$	Salicylate	313.0565	313.0548	8.08
19	Naringin	$C_{27}H_{32}O_{14}$	Non-methoxylated flavanone glycoside	579.1719	579.1658	8.19
20	Diosmin	$C_{28}H_{32}O_{15}$	Methoxylated flavonoid glycoside	607.1668	607.1636	8.21
21	Diosmetin-glucoside	$C_{22}H_{22}O_{11}$	Methoxylated flavone glycoside	461.1089	461.1079	8.25
22	Hesperidin	$C_{28}H_{34}O_{15}$	Methoxylated flavonoid glycoside	609.1825	609.1781	8.27
23	Limonin-17-β-D-glucoside	$C_{32}H_{42}O_{14}$	Limonoid	649.2502	649.2449	8.52
24	Didymin	$C_{28}H_{34}O_{14}$	Methoxylated flavonoid glycoside	593.1876	593.185	8.65
25	Nomilinic acid-17-β-D-glucoside	$C_{34}H_{48}O_{16}$	Limonoid	711.2870	711.2806	8.75
26	Nomilinic acid-β-glucopiranoside	$C_{34}H_{46}O_{15}$	Limonoid	693.2764	693.2693	8.88

27	lysoPE(18:2)	$C_{23}H_{44}NO_7P$	Lysophospholipid	476.2783	476.2738	9.50
28	lysoPE(18:2) isomer	$C_{23}H_{44}NO_7P$	Lysophospholipid	476.2783	476.2752	10.24
29	Limonin	$C_{26}H_{30}O_8$	Limonoid	515.1923	515.1863 (M+FA-H)	10.45
30	lysoPC(18:2) isomer	$C_{26}H_{50}NO_7P$	Lysophospholipid	564.3307	564.3317 (M+FA-H)	10.70
31	lysoPE(18:3)	$C_{23}H_{42}NO_7P$	Lysophospholipid	474.2626	474.2592	13.15
32	lysoPC(16:0)	$C_{24}H_{50}NO_7P$	Lysophospholipid	540.3307	540.3284 (M+FA-H)	13.19
33	lysoPE(18:3) isomer	$C_{23}H_{42}NO_7P$	Lysophospholipid	474.2626	474.2675	13.59
34	lysoPS(18:2)	$C_{24}H_{44}NO_9P$	Lysophospholipid	520.2681	520.2585	13.85
35	lysoPE(16:0)	$C_{21}H_{44}NO_7P$	Lysophospholipid	452.2783	452.2747	13.91

Table 3. Composition of TNVs. The table includes molecular formula, chemical class, retention time (Rt, min), and experimental and calculated m/z in negative ion mode.

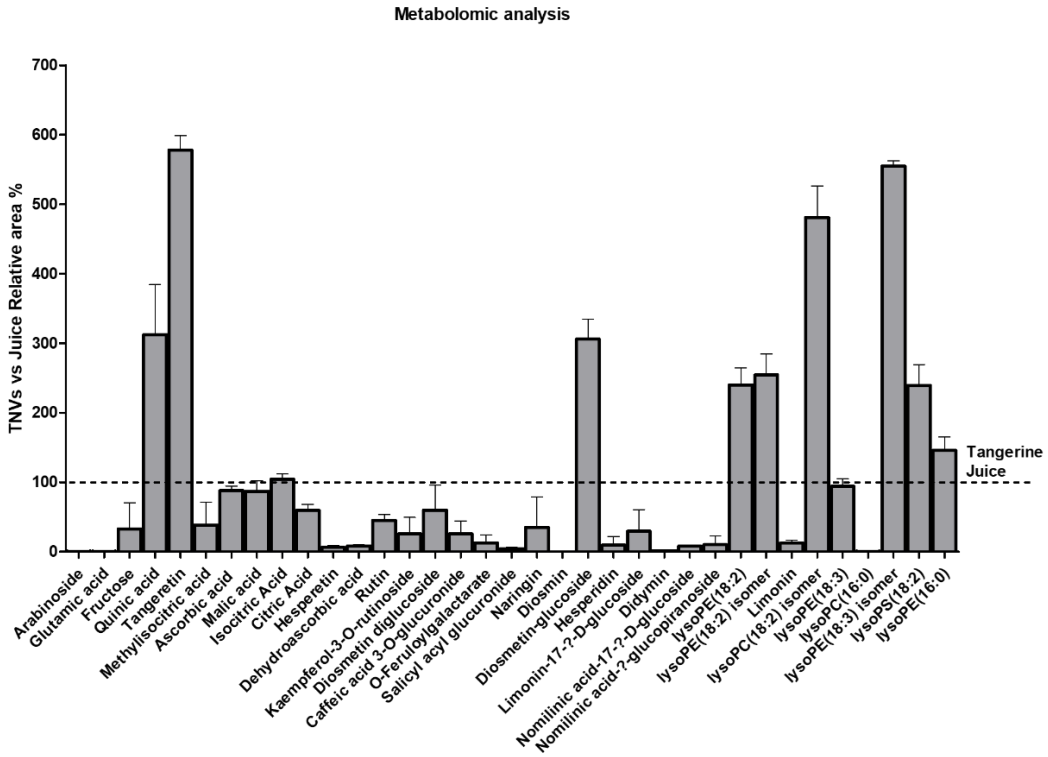

Figure 11. Metabolomic characterization of TNVs. Relative area % metabolites into TNVs versus Juice (n=2).

4.2. TNVs Can Be Internalized by Target Cells without Affecting their Viability

To test the safety of non-modified TNVs on normal and cancer cell lines we selected HS5 (human stromal cells), HDFα (human dermal fibroblasts), THLE2 (human hepatocyte), SW480 (human colorectal cancer cells), and Caco-2 (human colorectal adenocarcinoma cells) cells and treated them with increasing doses of TNVs (1, 5, 10, 25 μg/ml). Following 24 and 48 h of treatment with TNVs, we analyzed the cell viability of target cells by using MTT assay and we observed that TNVs did not alter the cell viability (Figure 12A). To ensure that colorectal cancer cells were

able to internalize TNVs, we labeled them with PKH-26 and treated SW480 for 2 h. Also, we monitor the TNV internalization in Caco-2 cells that, although originally derived from colon carcinoma, has been widely used as a model of intestinal epithelial barrier for their differentiation ability and low aggressiveness (90,91). Fluorescence microscopy analysis revealed that both cell lines internalized the vesicles, however the signal is higher in the most aggressive cell line SW480 (Figure 12B); this is a key element in the development of targeted therapies that aim to maximize treatment efficacy and minimize side effects.

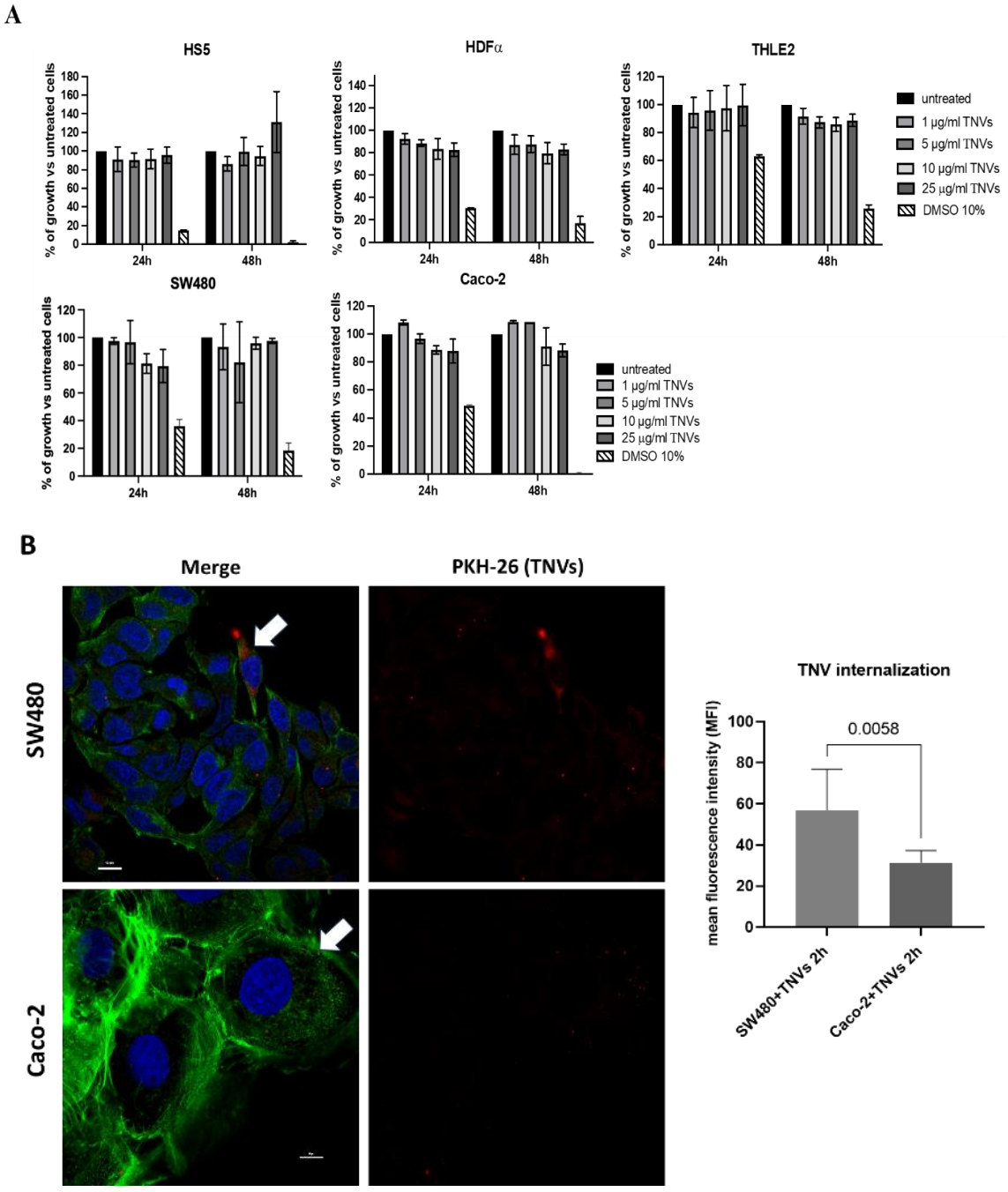

Figure 12: (A) TNVs did not affect the viability of normal and cancer cells. MTT assay of HS5, HDFα, THLE2, SW480 and Caco-2 cells treated with different doses of TNVs (1, 5, 10, 25 µg/ml) for 24 and 48 h. Cells were also

treated with 10% DMSO as positive control of cell death. (B) TNV internalization in SW480 and Caco-2 after 2 hours treatment; TNVs were stained with PKH26 (in red), actin with actin green (in green), and nuclei with Hoechst (in blue). Scale bars are 10µm. The histogram reports the mean fluorescence intensity (MFI) calculated based on cell surface. Data are represented as mean ±SD.

4.3. TNVs Can Be Loaded with siRNA through Electroporation

To test the possibility to use TNVs as natural nano-vehicles for drug delivery we selected the siRNA for DDHD1 since we previously reported that DDHD1 is involved in colorectal cancer cell proliferation and survival (79). First, we labeled scrambled- and DDHD1-siRNAs with Cy3 to follow the tracking of siRNA in the following experiments. Once we labeled DDHD1-siRNA, we electroporated 25 µg of TNVs with different amounts (20, 50, 100, 200 pmol) of Cy3-scrambled-siRNA or Cy3-DDHD1-siRNA (Figure 7). To confirm that the electroporation protocol did not alter TNVs' structure and size, we performed NTA, DLS, western blot, and AFM. As shown in Figure 13A, the size distribution measured by NTA was similar to the result shown in Figure 13A. Electroporated TNVs had a mean size of 216 nm ± 9 nm and a mode of 143 nm ± 7 nm. Analogous results are obtained by DLS (Figure 13B), which displays a z-average size of 214 ± 2 nm, a mode of 163 ± 2 nm, and a polydispersity index of 0.31. While particle concentration measured by NTA was unchanged between unloaded and electroporated TNVs, the total scattered intensity measured by DLS, which is proportional to the concentration, is lowered by one order of magnitude upon electroporation. Since DLS is anyhow able to capture the entire range of size distribution, this observation warns that the electroporation process may have induced the rupture/aggregation of some TNVs that were then removed from the solution by centrifugation; indeed, samples are mildly centrifuged before DLS experiments, which is the standard procedure for dust removal.

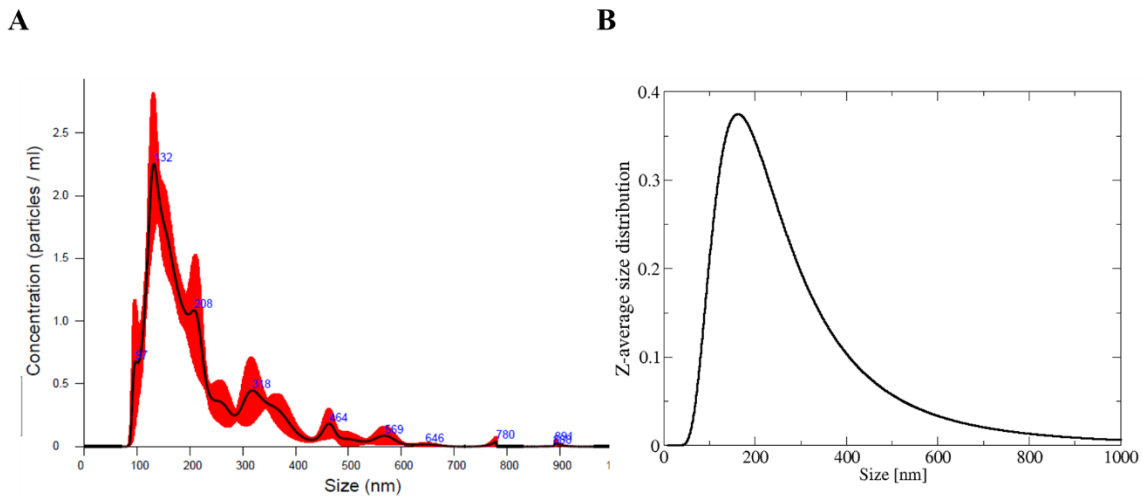

Figure 13. Cy3-siRNAs loading in TNVs through electroporation. (A) Size distribution of electroporated TNVs obtained through NTA. (B) Size distribution of electroporated TNVs obtained through DLS.

Through western blot, the presence of HSP70 was detected in electroporated TNVs (Figure 14A). The AFM images (Figure 14B) showed similar but less numerous objects to those in Figure 9A and Figure 10B (2.3 TNVs/µm2 for TNVs vs 1.4 TNVs/µm2 for electroporated TNVs), in accord with DLS measurements. Overall, these data demonstrated that the selected electroporation protocol did not impair the structure of TNVs.

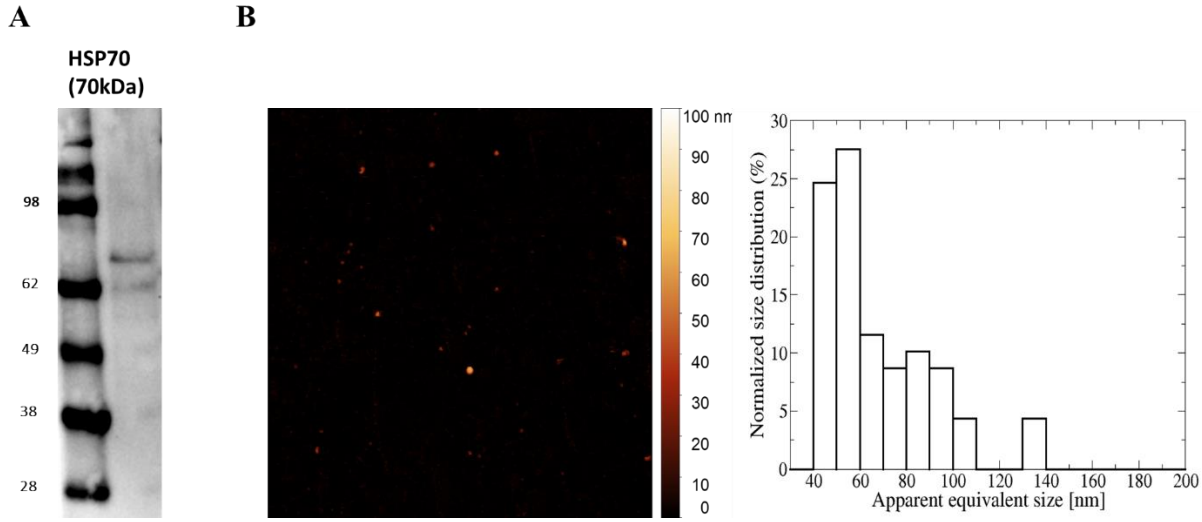

Figure 14. Cy3-siRNAs loading in TNVs through electroporation. (A) Western blot analysis of HSP70 in electroporated TNVs. (B) Representative AFM image (5 x 5 µm2) of electroporated TNVs (left panel) and the related statistical analysis (right panel)

To investigate the yield of Cy3-siRNAs loaded in TNVs, we measured the fluorescent signal of both Cy3-siRNA TNVs and of the supernatant obtained after the centrifugation to separate TNVs from the electroporation buffer (see Materials & Methods). As shown in Figure 15, the fluorescent signal was proportional to the amount (pmol) of Cy3-siRNA loaded in the TNVs. Furthermore, we detected fluorescence also in the supernatant, suggesting that the loading efficiency was not 100%. The ratio between the amount of Cy3-siRNA in the supernatant and those in TNVs showed that our loading efficiency is 13%.

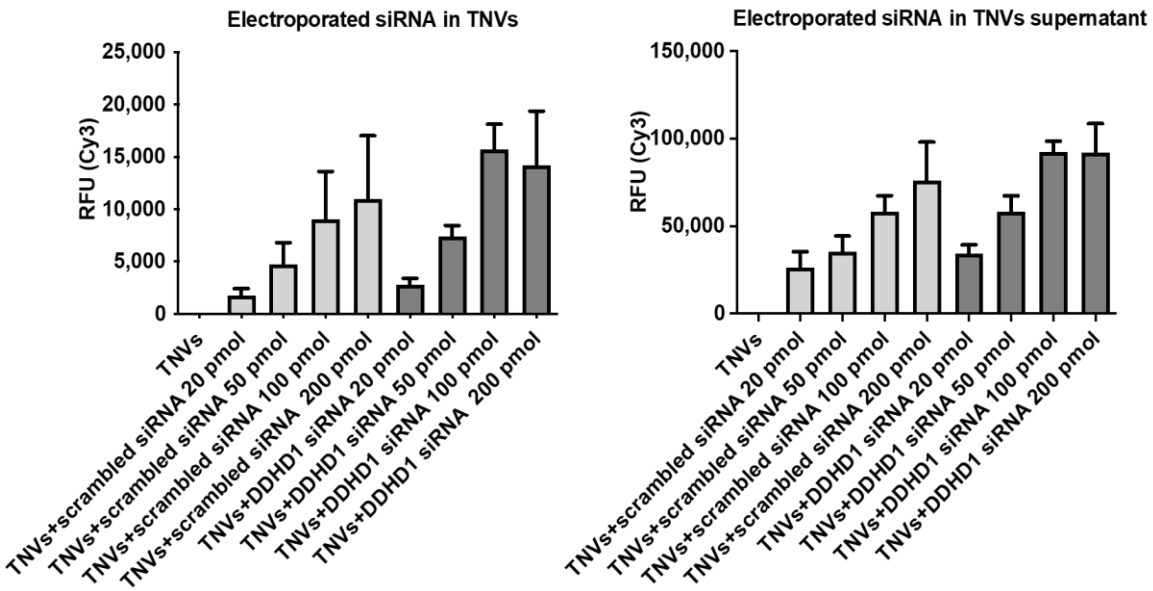

Figure 15. Cy3-siRNAs loading in TNVs through electroporation. The measurement of the fluorescent signal of Cy3-siRNA TNV pellet and supernatant was carried out with the plate reader (n=2-3).

Finally, to confirm that Cy3-siRNA was internalized in TNVs and not just attached to their surface, we removed not internalized RNAs by RNase treatment and then measured the fluorescent signal. As shown in Figure 16, the fluorescent signal of RNase-treated TNVs was comparable to the signal of untreated TNVs, demonstrating that our electroporation protocol determined the internalization of siRNA inside TNVs; the slight decrease of the fluorescence signal in RNase-treated TNVs may suggest that small amount of siRNA is on TNV surface. Overall, these data demonstrated that we successfully loaded DDHD1-siRNA inside TNVs through electroporation.

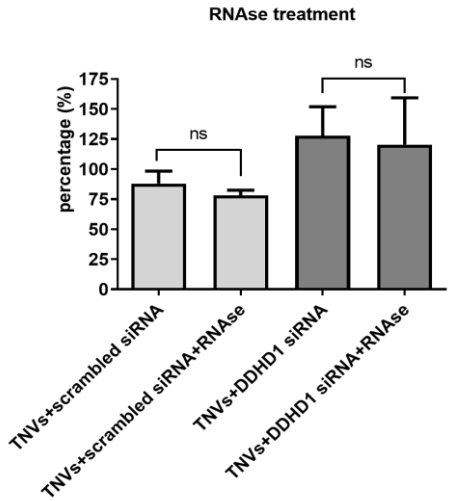

Figure 16. Cy3-siRNAs loading in TNVs through electroporation. The measurement of the fluorescent signal of Cy3-siRNA TNVs treated with RNase was carried out with the plate reader (n=3).

4.4. TNVs Delivered DDHD1-siRNA in Target Cells and Affected DDHD1 Expression

To verify whether the Cy3-siRNA TNV complex was internalized by human tumor cells, we incubated SW480 cells with Cy3-DDHD1-siRNA TNVs and analyzed them at confocal microscope. As shown in Figure 17A, Cy3-DDHD1-siRNA TNVs were internalized by target cells after 24 h of incubation. To confirm the confocal microscope analysis, we treated SW480 cells with Cy3-scrambled-siRNA TNVs and Cy3-DDHD1-siRNA TNVs for 24 h; at the end of the treatment the cell culture medium was removed, cells were washed twice in PBS to remove the non-internalized vesicle-siRNA complex, fresh PBS was added and then the fluorescent signal was measured at glomax. We observed that the fluorescent signal was directly proportional to the amount (pmol) of siRNA loaded in TNVs (Figure 17B).

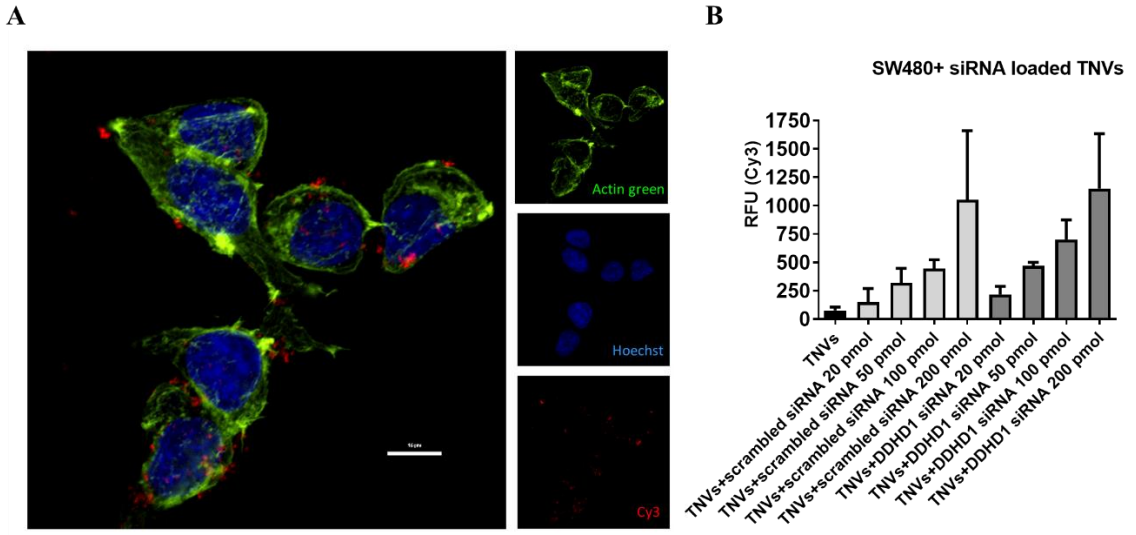

Figure 17. TNVs transfer DDHD1-siRNA into target cells thus downregulating DDHD1 expression. (A) Confocal microscopy analysis of SW480 cells incubated for 24 h with Cy3-DDHD1-siRNA TNVs (blue = nuclei, green = actin, red = Cy3-siRNA). (B) Cy3 fluorescence quantification of SW480 cells incubated for 24 h with TNVs, scrambled-siRNA TNVs, and DDHD1-siRNA TNVs (n=3).

Once we assessed that TNVs were able to successfully transfer siRNAs into target cells, we tested the function of siRNA-TNV complex on the modulation of DDHD1 in colorectal cancer cells. SW480 cells were treated with both DDHD1-siRNA TNV pellet and supernatant for 48 h and then we analyzed the gene expression of DDHD1. The obtained results showed that the treatment with DDHD1-siRNA TNVs supernatant did not affect DDHD1 gene expression. On the other hand, the treatment with DDHD1-siRNA TNV pellet downregulated DDHD1 gene expression in SW480 cells (Figure 18A); this reduction is comparable to that observed in SW480 transfected with DDHD1-siRNA using the commercially available transfection reagent HiPerFect (Figure

18B). The downregulation of DDHD1 was confirmed also at the protein level: western blot analysis demonstrated that the protein level of DDHD1 in SW480 cells treated with DDHD1-siRNA TNV pellet was lower compared to the control condition and cells treated with DDHD1-siRNA TNV supernatant (Figure 18C).

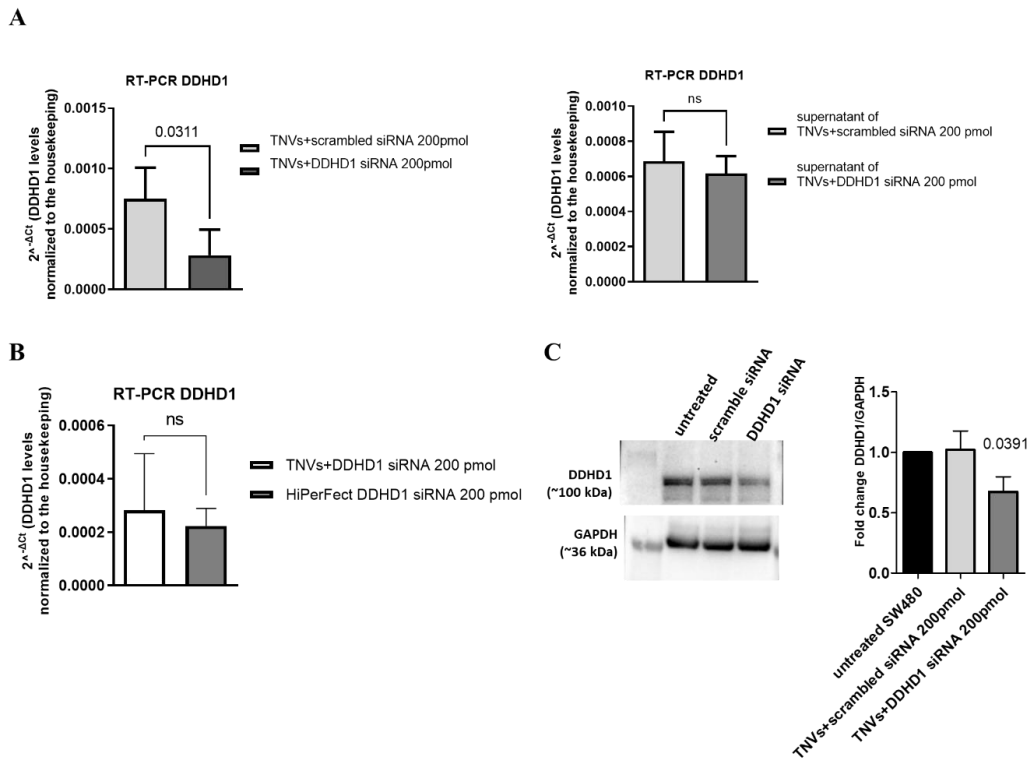

Figure 18. TNVs transfer DDHD1-siRNA into target cells thus downregulating DDHD1 expression. (A) The gene expression level of DDHD1 in SW480 cells treated with scrambled-siRNA TNVs and DDHD1-siRNA TNVs pellets (left panel, n=4) and supernatants (right panel, n=5) for 48 h. Value are plotted as the mean ±SD of the level of the target gene normalized to the housekeeping. (B) The gene expression level of DDHD1 in SW480 cells treated with DDHD1-siRNA TNV pellets or transfected with DDHD1-siRNA for 48 h using HiPerFect. Value is plotted as the mean ±SD of the level of the target gene normalized to the housekeeping. (n=4). (E) Western blot analysis of DDHD1 protein levels in SW480 cells treated with TNVs- scrambled-siRNA TNVs and DDHD1-siRNA TNVs (n=3).

The TNV-siRNA- mediated downregulation of DDHD1 revealed a trend of reduction in cell viability of 17% and 23% in cells treated with TNVs loaded respectively with 200 and 400 pmoli of DDHD1 siRNA (Figure 19).

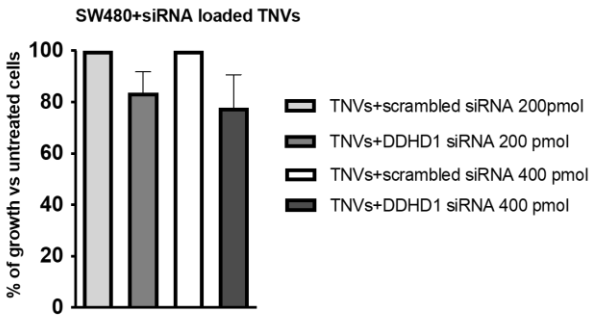

Figure 19. TNVs transfer DDHD1-siRNA into target cells thus downregulating DDHD1 expression. (A) MTT assay of SW480 cells treated for 48 h with scrambled-siRNA TNVs and DDHD1-siRNA TNVs (n=2).

CHAPTER 5

Discussion

Studies on the impacts and use of plant nanovesicles are quickly increasing. The potential to use plant nanovesicles as drug delivery systems for the treatment of various diseases, such as cancer and inflammation, has also been studied in recent years. (92-96). The ability of plant nanovesicles to be internalized into mammalian cells is the primary factor contributing to the feasibility of using them as therapeutic carriers. (97,98). Moreover, their lack of potential toxicity for humans (99), their biocompatibility, and their biodegradability make them attractive candidates for drug delivery. According to the findings of our study, homogeneous populations of nanovesicles with EV-like size, shape, and protein content were isolated from tangerine juice. Proteomic analysis highlights the presence of heat shock proteins HSP70, HSP90. These findings align with other studies that have reported the presence of heat shock proteins in plant-derived EVs. For instance, a study by Rutter and Innes (29) on Arabidopsis EVs also identified HSP70 and HSP90, highlighting their conserved roles across different species in maintaining protein homeostasis and aiding in the stress response mechanisms of EVs. Tetraspanins, another significant finding in our study, are a family of transmembrane proteins. This is consistent with the findings of Rutter and Innes (29) and later confirmed by Pinedo et al. (26), who demonstrated that tetraspanins are not only present in mammalian EVs but also play a crucial role in plant-derived EVs, supporting their involvement in diverse biological processes including immune responses and cell signaling. Metabolomic analysis allows us to observe that TNVs are abundant in lipids, limonoids, and flavonoid derivatives. Many of these compounds have been extensively investigated for their possible therapeutic role in several cancer types, including breast, lung, prostate, and colon cancer. Among them, Tangeretin (100-102), Hesperetin (103,104), Rutin (105,106), and Naringenin (106) are already known for their considerable anti-cancer properties and give TNVs intrinsic valuable qualities, intriguing for future studies. In line with previous findings, showing that nanovesicles derived from plants do not affect normal cell growth (107,108), here we found that TNVs have no cytotoxic effects on different normal cell lines; in our study, TNVs, at the tested concentration, do not even alter the viability of colon cancer cells. These results highlighted the possibility to use them as drug vehicles. Notably, our observations reveal a higher

internalization of TNVs by the aggressive colorectal cancer cell lines SW480 when compared to Caco-2 cells. In the context of utilizing TNVs as drug delivery vehicles, this process may enhance the targeted delivery of therapeutic agents to cancer cells, minimizing the impact on healthy tissues and resulting in a more effective and selective therapeutic outcome. Given their biocompatibility and safety, several studies have been conducted to identify a successful method for drug loading in plant nanoparticles (93,97,109,110). Nowadays, sonication and co-incubation are the most used approaches for drug loading in plant nanoparticles (36,92,99,111). For instance, Garaeva et al. loaded grapefruit-derived nanovesicles with bovine serum albumin and heat shock protein 70 through a sonication technique (98). Other groups used co-incubation methods to load nanoparticles isolated from aloe (108), acerola (109), and lemon (97). To our knowledge, this is the first study in which electroporation has been used for siRNA loading in plant nanoparticles. Indeed, before selecting electroporation as an eligibility method for TNVs loading, we tried also co-incubation and sonication; however, neither of these two approaches allowed us to effectively load the nanovesicles (data shown below).

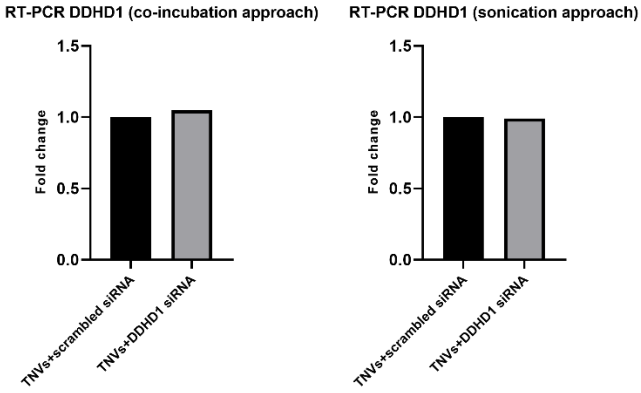

This encouraged us to draw attention to the distinctive characteristics of nanoparticles from various plant matrices, such as diverse lipid compositions (112), thus explaining the different loading approaches that have been used. In this study, we effectively loaded siRNA into TNVs using the electroporation method; the transfection efficiency was found to be 13%. In this regard, prior research showed that our findings were consistent with the transfection effectiveness of the electroporation loading technique for animal nanovesicles (113,114). In 2022, Zhang et al. investigated the effect of miR-665-loaded EVs on osteosarcoma. By using electroporation, they loaded EVs with miR-665 and this complex can prevent the progression of osteosarcoma in vitro and in vivo (115). Another study aimed to repair Spinal Cord Injury (SCI) by loading siRNA in engineered nanovesicles through electroporation. Overall, EVs-siRNA targeted the injured spinal cord in SCI mice and elicited significant functional recovery (116). To study the anticancer effect of FU-5 in colon cancer, FU-5, and miR-21 have been electroporated into EVs. In the last study,

the researchers found that the EV-based FU-5 and mir-21 systems can effectively facilitate cellular uptake; they found that the complex re-duces tumor proliferation and increases apoptosis (117). Here, we demonstrated that the TNVs-siRNA complex has functional properties. We demonstrated that DDHD1-siRNA is successfully transferred into target cells by TNVs, thereby reducing DDHD1 expression.

CHAPTER 6

Preliminary Results on Mammalian EVs as Delivery Systems

Considering the results obtained and described in the previous section, suggesting that siRNA can be loaded into tangerine-derived nanovesicles using the electroporation method, to test whether this approach can be applied also to mammalian vesicles, we decided to use EVs purified from human embryonic kidney cells (HEK293T). In particular, we focused on loading onco-suppressor microRNAs in EVs and testing the functionality of the complex on thyroid cancer cell lines. To increase the cell-specific targeting of the EV-miRNA complex, we decorated EV with Hyaluronic acid (HA), since cancer cells overexpress its receptor, CD44.

6.1. Materials and Methods

6.1.1. Cell Culture

Human Embryonic Kidney 293T (HEK293T) cells was obtained from ATCC (Manassas, VA, USA). HEK293T cells were cultured in Dulbecco's modified Eagle's medium (DMEM; Euroclone, UK) with 10% fetal bovine serum ultra-centrifuged at 100,000 × g for 1 h and 45 min in a Type 70 Ti, fixed angle rotor was filtered at 0.22 μm pore filter (FBS, Euroclone), 100 U/mL of penicillin, 100 U/mL of streptomycin, and 2 mM L-glutamine (Euroclone).

The human Follicular thyroid carcinoma (TT2609-CO2) was obtained from ATCC (Manassas, VA, USA) and was cultured in RPMI 1640 medium (Euroclone, UK) supplemented with 20% fetal bovine serum (FBS, Euroclone), 1% of Sodium Pyruvate, 1% Insulin-Transferrin-Selenium Supplement, and 2 mM L-glutamine (Euroclone), 100 U/ml penicillin and 100 μg/ml streptomycin (Euroclone).

Anaplastic thyroid carcinoma (CAL-62) was obtained from ATCC (Manassas, VA, USA) and was cultured in DMEM medium (Euroclone, UK) supplemented with 10% fetal bovine serum (FBS, Euroclone), 2 mM L-glutamine (Euroclone), 100 U/ml penicillin and 100 μg/ml streptomycin (Euroclone).

Thyroid carcinoma (B-CPAP) was obtained from ATCC (Manassas, VA, USA) and was cultured in RPMI 1640 medium (Euroclone, UK) supplemented with 20% fetal bovine serum (FBS, Euroclone), 2 mM L-glutamine (Euroclone), 100 U/ml penicillin and 100 µg/ml streptomycin (Euroclone).

6.1.2. Isolation of Extracellular Vesicles from HEK293T

HEK293T cells were cultured in T175 flasks for a duration of 48 hours under standard conditions. The Conditioned medium (CM) was collected using differential centrifugation, and ultra-centrifugation. The CM was sequentially centrifuged at 300 × g for 5 minutes, 3,000 × g for 15 minutes, and centrifuged at 10,000 × g for 30 minutes, then the supernatant was ultra-centrifuged at 100.000 × g for 1 hour 45 minutes. EV quantification was determined with the Bradford assay (Pierce, Rockford, IL, USA).

6.1.3. Decoration of HEK293T EVs with Hyaluronic Acid (HA)

Hyaluronic Acid (HA) conjugated to Alexa488 was prepared by dissolving 1 mg of powders in 100 µl of H2O to achieve a starting solution concentration of 10 µg/µl. EVs (100 µg) were incubated overnight with 6 µg of HA. Following overnight incubation, centrifugation at 14,000 rpm for 10 minutes, removal of supernatant, washing with 200 µl of PBS, and resuspension of the pellet in 100 µl of PBS were carried out.

6.1.4. Confocal Microscopy

To investigate the internalization of EV-HA by TT2609-CO2 cells, 100 µg of EV, previously decorated with HA, were labeled with the lipophilic dye PKH26. TT2609-CO2 cells were seeded at a concentration of 500,000 cells per well and then incubated with the EV-HA for 1 hour at 37°C. Following treatment, to verify the EV-HA internalization, cells were fixed with PFA 4% and permeabilized with TritonX-100. Cellular actin was stained with Actin Green (Molecular Probes, Life Technologies, Carlsbad, CA, USA), while Nuclei with Hoechst (Molecular Probes, Life Technologies, Carlsbad, CA, USA). The samples were analyzed by confocal microscopy (Nikon A1, Amsterdam, Netherlands).

6.1.5. Loading of microRNA mimics in EV-HA

Based on the results obtained in the PDNVs, selected miRNA mimics were loaded in EVs through the electroporation protocol developed and then the sample was centrifuged at 14,000 x g for 20 min to remove the not-loaded miRNAs (Described in paragraph 3.14). Through collaboration

with Dr. Forte (IOM, Catania) and an extensive literature review, two microRNAs (miR-146a and miR-199a) were identified among the numerous for their anti-tumor capabilities (118-120). Loading was performed by mixing EVs (50 µg/ml) with microRNAs (200 pmol of scrambled or miRNA) in an electroporation buffer. The miRNA-loaded EVs were decorated with 3 µg of HA as described in paragraph 6.1.2. A schematic description of the protocol is represented in Figure 20.

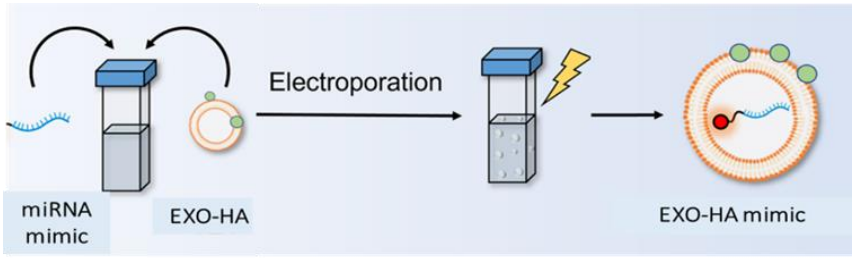

Figure 20: miRNA mimic loading in EV-HA through electroporation.

6.1.6. RNA Isolation and Real-Time PCR

TT2609-CO2, CAL-62, and B-CPAP cells were seeded in 12-well plates at 400,000 cells/well. After 24 h, 50 µg of the complexes EV HA+ miRNA mimic or EV HA+ miRNA scrambled were incubated with the three cell lines for 24 hours. Total RNA was extracted using Illustra^{TM} RNA spin mini-RNA isolation Kit according to the manufacturer's instructions (GE Healthcare, Little Chalfont, Buckinghamshire, UK). The specific microRNAs were converted in cDNA using the TaqMan™ MicroRNA Reverse Transcription Kit (Applied Biosystems, Foster City, CA, USA). Then, to evaluate the levels of miR-146a and miR-199a RT-QPCR was performed.

6.2. Preliminary Results

6.2.1. Decoration of HEK293T EVs with Hyaluronic Acid (HA)

Thanks to the collaboration with Prof. Cavallaro and Prof. Palumbo of the University of Palermo, we first tested 3 different polymers of Hyaluronic acid (HA), conjugated with the fluorescent dye Alexa 488: HA 10KDa, HA 100KDa, HA 100KDa-C18.

EVs were incubated with HA overnight. Fluorescence quantification using Glomax showed a stronger signal in the EV-HA 100KDa-C18-Alexa488 complex, indicating successful decoration with this molecule (Figure 21). Based on these results, HA 100KDa-C18-Alexa488 was selected for further experiments.

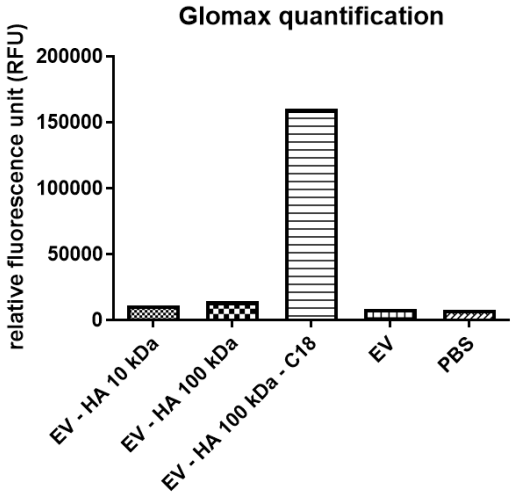

Figure 21: fluorescence quantification of HA in EV.

6.2.2. EV-HA are Internalized by Target Cells

To ensure that the decoration with HA did not alter the ability of EVs to interact with target cells, we labeled them with PKH-26. The TT2609-CO2 cell line was incubated with HA-EVs for 3 h. As illustrated in Figure 22, confocal microscope analysis confirmed that EVs, decorated with HA, were internalized by cancer cells.

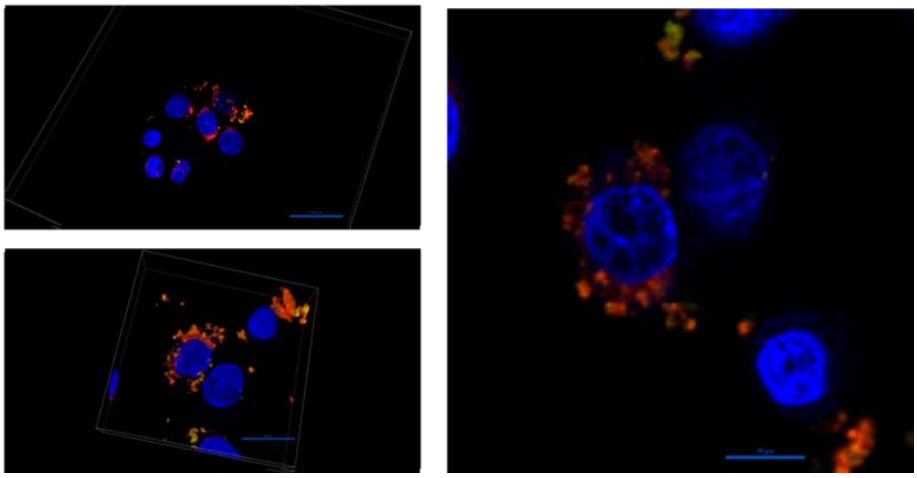

Figure 22: Confocal microscopy analysis of TT2609-CO2 cells incubated for 3h with EV were decorated with HA. (blue= nuclei, red= EV).

6.2.3. Expression Level of microRNA

Treatment of TT2609, CAL-62, and B-CPAP cells with the complex consisting of EV, with or without HA, loaded with miR146a and miR199a (EV+mimic199a+146a) or with miRNA scrambled, resulted in elevated levels of both miRNAs compared to the control group treated with EV loaded with a scrambled sequence (EV+SCR). Furthermore, in most instances, a more pronounced increase in the expression of miR146a and miR199a was observed in cells treated with the HA-decorated complex (EV-HA+mimic199a+146a) compared to cells treated with non-

decorated EVs loaded with miR199a and miR146a (EV+miRNA199a+146a), indicating that HA enhances the delivery efficiency of miRNAs to target cells (Figure 23A-C).

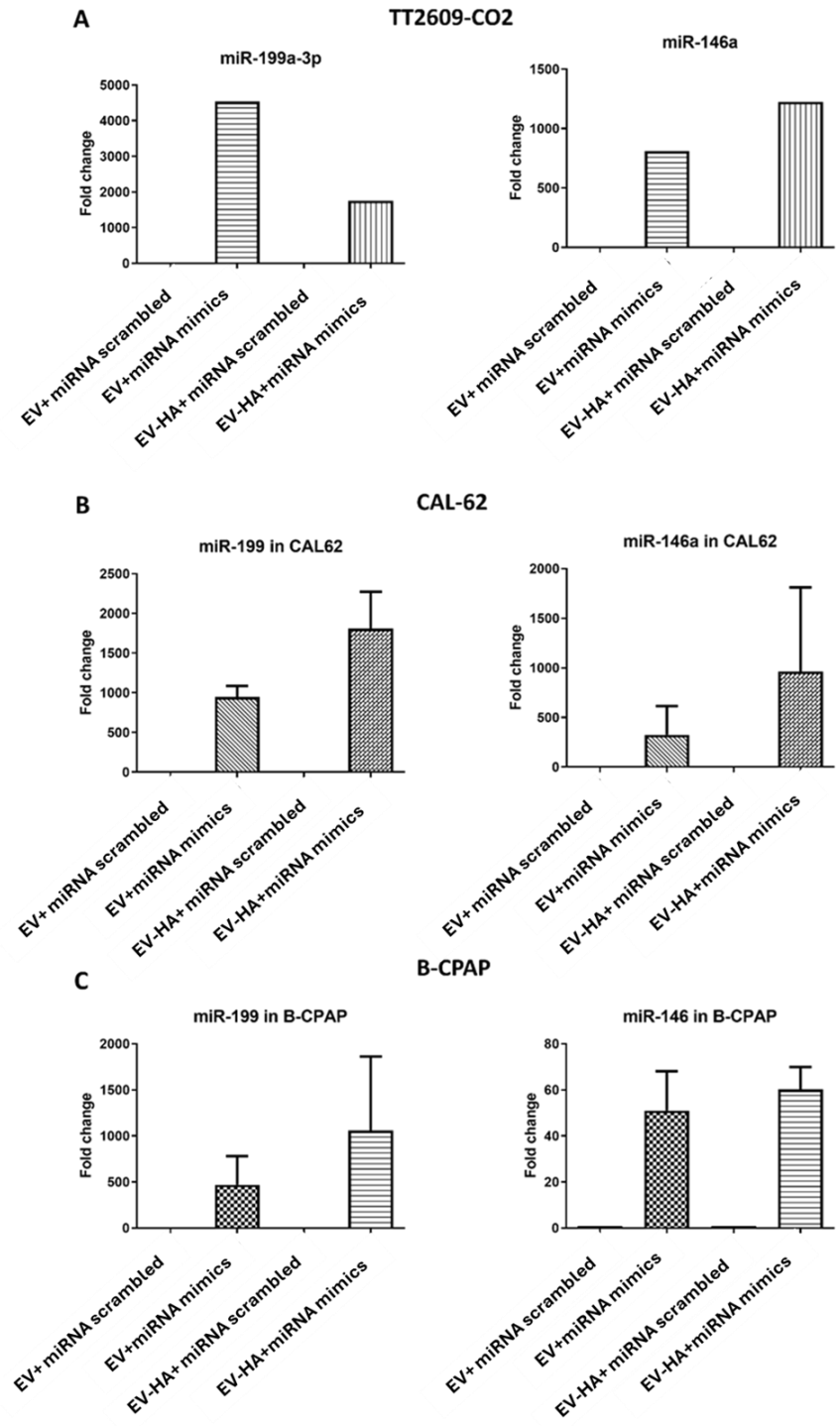

Figure 23: miR199/miR146 levels were evaluated through Real-Time PCR in (A) TT2609-CO2, (B) CAL-62, and (C) B-CPAP cells after incubation with the complexes EV-miRNAs.

6.3. Conclusion and Final Perspectives

Three-dimensional (3D) cultures of tumor cells that best mimic the cellular environment have emerged as scientifically accurate and low-cost tumor models for the preclinical screening of new therapeutics. Various tumor cells can spontaneously assemble into spheroids under appropriate culture conditions that favor cell-cell and cell-matrix interactions; under such conditions, tumor cells can proliferate, aggregate, and differentiate (121). Therefore, such a system mimics many features of tumors in vivo, such as cell-cell and cell-matrix interactions, nutrient and oxygen gradients, and different layers of cell populations. In a 2020 study, eight different thyroid carcinoma cell lines were observed to readily form spheroids sensitive to common drug treatments (122).

Therefore, considering the preliminary results on the ability of HA-EVs to deliver exogenous miRNA to tumor cells, the next studies will be aimed at confirming what we observed in the 2D model in spheroids.

CHAPTER 7

Scientific Products

7.1. List of publications or other scientific products produced within the project and relevant to the topic

7.1.1. Scientific publications in journals

1. Tinnirello V, Zizzo MG, Conigliaro A, Tabone M, **Ganji NR**, Cicio A, Bressa C, Larrosa M, Rappa F, Vergilio G, Gasparro R, Gallo A, Serio RM, Alessandro R, Raimondo S. Industrial-produced lemon nanovesicles ameliorate experimental colitis-associated damages in rats via the activation of anti-inflammatory and antioxidant responses and microbiota modification. Biomed Pharmacother. 2024 Apr 2;174:116514. doi: 10.1016/j.biopha.2024.116514. Epub ahead of print. PMID: 38574618.

2. **Rabienezhad Ganji N**, Urzì O, Tinnirello V, Costanzo E, Polito G, Palumbo Piccionello A, Manno M, Raccosta S, Gallo A, Lo Pinto M, Calligaris M, Scilabra SD, Di Bella MA, Conigliaro A, Fontana S, Raimondo S, Alessandro R. Proof-of-Concept Study on the Use of Tangerine-Derived Nanovesicles as siRNA Delivery Vehicles toward Colorectal Cancer Cell Line SW480. Int J Mol Sci. 2023 Dec 30;25(1):546. doi: 10.3390/ijms25010546. PMID: 38203716; PMCID: PMC10779162.

3. Urzì O, Cafora M, **Ganji NR**, Tinnirello V, Gasparro R, Raccosta S, Manno M, Corsale AM, Conigliaro A, Pistocchi A, Raimondo S, Alessandro R. Lemon-derived nanovesicles achieve antioxidant and anti-inflammatory effects activating the AhR/Nrf2 signaling pathway. iScience. 2023 Jun 7;26(7):107041. doi: 10.1016/j.isci.2023.107041. PMID: 37426343; PMCID: PMC10329147.

4. Tinnirello V, **Rabienezhad Ganji N***, De Marcos Lousa C, Alessandro R, Raimondo S. Exploiting the Opportunity to Use Plant-Derived Nanoparticles as Delivery Vehicles. Plants (Basel). 2023 Mar 7;12(6):1207. doi: 10.3390/plants12061207. PMID: 36986896; PMCID: PMC10053153. (* Co-first authors).

5. Raimondo S, Urzì O, Meraviglia S, Di Simone M, Corsale AM, **Rabienezhad Ganji N**, Palumbo Piccionello A, Polito G, Lo Presti E, Dieli F, Conigliaro A, Alessandro R. Anti-inflammatory properties of lemon-derived extracellular vesicles are achieved through the inhibition of ERK/NF-κB signalling pathways. J Cell Mol Med. 2022 Aug;26(15):4195-4209. doi: 10.1111/jcmm.17404. Epub 2022 Jul 4. PMID: 35789531; PMCID: PMC9344827.

6. Urzì O, Gasparro R, **Ganji NR**, Alessandro R, Raimondo S. Plant-RNA in Extracellular Vesicles: The Secret of Cross-Kingdom Communication. Membranes (Basel). 2022 Mar 23;12(4):352. doi: 10.3390/membranes12040352. PMID: 35448322; PMCID: PMC9028404.

7.1.2. Abstracts and posters presented at scientific congresses

1. **Mechanisms of intercellular and inter-organismal communication via RNA**
   Poster title: Proof-of-concept study on the use of tangerine-derived nanovesicles as RNAi delivery vehicles toward mammalian cells
   September 2023, Paris
2. **95° Congresso della Società Italiana di Biologia Sperimentale (SIBS**
   Poster title: Proof-of-concept study on the use of tangerine-derived nanovesicles as siRNA delivery vehicles towards mammalian cell lines
   April 2023, Trieste
3. **XXVII SCHOOL OF PURE AND APPLIED BIOPHYSICS**
   Poster title: Proof-of-concept study on the use of tangerine-derived nanovesicles as siRNA delivery vehicles towards mammalian cell lines
   February 2023, Venice
4. **Supramed National meeting: Sustainable practice in medicinal chemistry**
   Abstract title: Plant-Derived Extracellular Vesicles as Drug Delivery Systems: A Proof Of Concept Study Using Tangerine Vesicles
   April 2022, Palermo
5. **Microscopy Conference**
   Abstract title: Isolation and characterization of Tangerine-derived extracellular vesicles
   2021, Italy

7.2. List of publications or products (carried out by the PhD st in collaboration within the time frame of the project) not related to the project

7.2.1. Scientific publications in journals

1. Kheirvari M, Lacy VA, Goudarzi H, **RabieNezhad Ganji N**, Kamali Ardekani M, Anbara T. The changes in cognitive function following bariatric surgery considering the function of gut microbiome. Obes Pillars. 2022 May 18;3:100020. doi: 10.1016/j.obpill.2022.100020. PMID: 37990721; PMCID: PMC10662092.

2. Amini, N., Najafi, S., **RabieNezhad Ganji, N**., Mirazi, N., Abbasalipourkabir, R. Effects of Black Raspberry Extract on the Oxidant-Antioxidant System Balance in an Animal Model of Diabetes. International Journal of BioLife Sciences (IJBLS), 2023; 2(1): 92-97. doi: 10.22034/jbs.2023.178667.

3. Hashemi, A., shabanzadeh, M., **Rabienezhad Ganji, N**., Sirati Moghaddam, P. Identification of EGFR Gene Exon 21 and 20 Mutations Based on the Method of PCR Sequencing in Paraffin Biopsy of Lung Cancer. International Journal of BioLife Sciences (IJBLS), 2023; 2(2): 242-252. doi: 10.22034/ijbls.2023.185495.

4. Dalghi, E., **RabieNezhad Ganji, N**. Exploring Oncology Research: From Molecular Discoveries to Translational Breakthroughs. International Journal of BioLife Sciences (IJBLS), 2023; 2(2): 173-180. doi: 10.22034/ijbls.2023.185484.

5. Ahmadi, A., **RabieNezhad Ganji, N**. AI-Driven Medical Innovations: Transforming Healthcare through Data Intelligence. International Journal of BioLife Sciences (IJBLS), 2023; 2(2): 132-142. doi: 10.22034/ijbls.2023.185475.

6. **Ganji, N. R***., Shabanzadeh, M., Sirati Moghaddam, P., & RabieNezhad Ganji, S. (2023). Cytotoxic effects of ibuprofen on cervical cancer (Hela) cells through induction of nitric oxide synthase2 (iNOS) gene expression. Journal of Biological Studies, 6(1), 169–177. https://doi.org/10.62400/jbs.v6i1.7777

7. Shabanzadeh, M., Sirati Moghaddam, P., RabieNezhad Ganji, S., **RabieNezhadganji, N***. The Effects of Estradiol Valerate and Progesterone on the Activity of Caspase-8 and -9 and Evaluating the Expression of BAX, BCL2, and P53 Genes in the Apoptosis Pathway of HT29 Cancer Cells in the Cell Culture. International Journal of BioLife Sciences (IJBLS), 2022; 1(4): 227-234. doi: 10.22034/jbs.2023.366590.1004.

CHAPTER 8

Bibliography

1. Sarkar, S., Patranabis, S. Emerging Role of Extracellular Vesicles in Intercellular Communication in the Brain: Implications for Neurodegenerative Diseases and Therapeutics. Cell Biochem Biophys (2024). https://doi.org/10.1007/s12013-024-01221-z

2. Yuki Takahashi, Yoshinobu Takakura, Extracellular vesicle-based therapeutics: Extracellular vesicles as therapeutic targets and agents, Pharmacology & Therapeutics, Volume 242, 2023, 108352, ISSN 0163-7258, https://doi.org/10.1016/j.pharmthera.2023.108352.

3. Ahmad S, Srivastava RK, Singh P, Naik UP, Srivastava AK. Role of Extracellular Vesicles in Glia-Neuron Intercellular Communication. Front Mol Neurosci. 2022 Apr 13;15:844194. doi: 10.3389/fnmol.2022.844194. PMID: 35493327; PMCID: PMC9043804.

4. Minakawa T, Yamashita JK. Versatile extracellular vesicle-mediated information transfer: intercellular synchronization of differentiation and of cellular phenotypes, and future perspectives. Inflamm Regen. 2024 Jan 15;44(1):4. doi: 10.1186/s41232-024-00318-5. PMID: 38225584; PMCID: PMC10789073.

5. Aloi N, Drago G, Ruggieri S, Cibella F, Colombo P, Longo V. Extracellular Vesicles and Immunity: At the Crossroads of Cell Communication. Int J Mol Sci. 2024 Jan 18;25(2):1205. doi: 10.3390/ijms25021205. PMID: 38256278; PMCID: PMC10816988.

6. Yokoi A, Ochiya T. Exosomes and extracellular vesicles: Rethinking the essential values in cancer biology. Semin Cancer Biol. 2021 Sep;74:79-91. doi: 10.1016/j.semcancer.2021.03.032. Epub 2021 Mar 31. PMID: 33798721.

7. Correa R, Caballero Z, De León LF, Spadafora C. Extracellular Vesicles Could Carry an Evolutionary Footprint in Interkingdom Communication. Front Cell Infect Microbiol. 2020 Mar 3;10:76. doi: 10.3389/fcimb.2020.00076. PMID: 32195195; PMCID: PMC7063102.

8. Couch Y, Buzàs EI, Di Vizio D, Gho YS, Harrison P, Hill AF, Lötvall J, Raposo G, Stahl PD, Théry C, Witwer KW, Carter DRF. A brief history of nearly EV-erything - The rise and rise of extracellular vesicles. J Extracell Vesicles. 2021 Dec;10(14):e12144. doi: 10.1002/jev2.12144. PMID: 34919343; PMCID: PMC8681215.

9. Bazzan E, Tinè M, Casara A, Biondini D, Semenzato U, Cocconcelli E, Balestro E, Damin M, Radu CM, Turato G, Baraldo S, Simioni P, Spagnolo P, Saetta M, Cosio MG. Critical Review of the Evolution

of Extracellular Vesicles' Knowledge: From 1946 to Today. Int J Mol Sci. 2021 Jun 15;22(12):6417. doi: 10.3390/ijms22126417. PMID: 34203956; PMCID: PMC8232679.

10. Théry, C., Witwer, K. W., Aikawa, E., Alcaraz, M. J., Anderson, J. D., Andriantsitohaina, R., & AC, N. (2018). Minimal information for studies of extracellular vesicles 2018 (MISEV2018): a position statement of the International Society for Extracellular Vesicles and update of the MISEV2014 guidelines. Journal of extracellular vesicles, 7(1), 1535750.

11. Coumans, F. A., Brisson, A. R., Buzas, E. I., Dignat-George, F., Drees, E. E., El-Andaloussi, S., & Lacroix, R. (2017). Methodological guidelines to study extracellular vesicles. Circulation research, 120(10), 1632-1648.

12. Clarke-Bland CE, Bill RM, Devitt A. Emerging roles for AQP in mammalian extracellular vesicles. Biochim Biophys Acta Biomembr. 2022 Mar 1;1864(3):183826. doi: 10.1016/j.bbamem.2021.183826. Epub 2021 Nov 27. PMID: 34843700; PMCID: PMC8755917.

13. Zhang, Y., Liu, Y., Liu, H. et al. Exosomes: biogenesis, biologic function and clinical potential. Cell Biosci 9, 19 (2019). https://doi.org/10.1186/s13578-019-0282-2.

14. Ståhl AL, Johansson K, Mossberg M, Kahn R, Karpman D. Exosomes and microvesicles in normal physiology, pathophysiology, and renal diseases. Pediatr Nephrol. 2019 Jan;34(1):11-30. doi: 10.1007/s00467-017-3816-z. Epub 2017 Nov 27. PMID: 29181712; PMCID: PMC6244861.

15. Chitti SV, Gummadi S, Kang T, Shahi S, Marzan AL, Nedeva C, Sanwlani R, Bramich K, Stewart S, Petrovska M, Sen B, Ozkan A, Akinfenwa M, Fonseka P, Mathivanan S. Vesiclepedia 2024: an extracellular vesicles and extracellular particles repository. Nucleic Acids Res. 2024 Jan 5;52(D1):D1694-D1698. doi: 10.1093/nar/gkad1007. PMID: 37953359; PMCID: PMC10767981.

16. Ali, N.B.; Abdull Razis, A.F.; Ooi, D.J.; Chan, K.W.; Ismail, N.; Foo, J.B. Theragnostic Applications of Mammal and Plant-Derived Extracellular Vesicles: Latest Findings, Current Technologies, and Prospects. Molecules 2022, 27, 3941. https://doi.org/10.3390/molecules27123941.

17. Jin Y, Ma L, Zhang W, Yang W, Feng Q, Wang H. Extracellular signals regulate the biogenesis of extracellular vesicles. Biol Res. 2022 Nov 26;55(1):35. doi: 10.1186/s40659-022-00405-2. PMID: 36435789; PMCID: PMC9701380.

18. Vietri M, Radulovic M, Stenmark H. The many functions of ESCRTs. Nat Rev Mol Cell Biol. 2020;21(1):25–42. doi: 10.1038/s41580-019-0177-4.

19. Mathieu M, Martin-Jaular L, Lavieu G, Thery C. Specificities of secretion and uptake of exosomes and other extracellular vesicles for cell-to-cell communication. Nat Cell Biol. 2019;21(1):9–17. doi: 10.1038/s41556-018-0250-9.

20. Suárez H., Gámez-Valero A., Reyes R., López-Martín S., Rodríguez M. J., Carrascosa J. L., et al. (2017). A bead-assisted flow cytometry method for the semi-quantitative analysis of Extracellular Vesicles. Sci. Rep. 7 (1), 11271. PMID: 28900146; PMCID: PMC5595788.

21. Welsh JA, Goberdhan DCI, O'Driscoll L, Buzas EI, Blenkiron C, Bussolati B, Cai H, Di Vizio D, et al. Minimal information for studies of extracellular vesicles (MISEV2023): From basic to advanced

approaches. J Extracell Vesicles. 2024 Feb;13(2):e12404. doi: 10.1002/jev2.12404. Erratum in: J Extracell Vesicles. 2024 May;13(5):e12451. PMID: 38326288; PMCID: PMC10850029.

22. Candelario KM, Steindler DA. The role of extracellular vesicles in the progression of neurodegenerative disease and cancer. Trends Mol Med. 2014 Jul;20(7):368-74. doi: 10.1016/j.molmed.2014.04.003. Epub 2014 May 14. PMID: 24835084; PMCID: PMC4083510.

23. Li Z, Wang X, Wang X, Yi X, Wong YK, Wu J, Xie F, Hu D, Wang Q, Wang J, Zhong T. Research progress on the role of extracellular vesicles in neurodegenerative diseases. Transl Neurodegener. 2023 Sep 11;12(1):43. doi: 10.1186/s40035-023-00375-9. PMID: 37697342; PMCID: PMC10494410.

24. Fang Y, Wang Z, Liu X, Tyler BM. Biogenesis and Biological Functions of Extracellular Vesicles in Cellular and Organismal Communication With Microbes. Front Microbiol. 2022 Feb 18;13:817844. doi: 10.3389/fmicb.2022.817844. PMID: 35250933; PMCID: PMC8895202.

25. Shahbazi R, Kalishwaralal K, Paul MK, Anto RJ. Editorial: Role of extracellular vesicles (EVs) in pathogenesis, diagnosis, therapeutic delivery, treatment and theranostic applications in cancer. Front Bioeng Biotechnol. 2023 Sep 15;11:1288806. doi: 10.3389/fbioe.2023.1288806. PMID: 37786406; PMCID: PMC10541950.

26. Pinedo M, de la Canal L, de Marcos Lousa C. A call for Rigor and standardization in plant extracellular vesicle research. J Extracell Vesicles. 2021 Apr;10(6):e12048. doi: 10.1002/jev2.12048. Epub 2021 Apr 27. PMID: 33936567; PMCID: PMC8077130.

27. Tinnirello V, Rabienezhad Ganji N, De Marcos Lousa C, Alessandro R, Raimondo S. Exploiting the Opportunity to Use Plant-Derived Nanoparticles as Delivery Vehicles. Plants (Basel). 2023 Mar 7;12(6):1207. doi: 10.3390/plants12061207. PMID: 36986896; PMCID: PMC10053153.

28. Alzahrani, F.A.; Khan, M.I.; Kameli, N.; Alsahafi, E.; Riza, Y.M. Plant-Derived Extracellular Vesicles and Their Exciting Potential as the Future of Next-Generation Drug Delivery. Biomolecules 2023, 13, 839. https://doi.org/10.3390/biom13050839.

29. Rutter B. D., Innes R. W. (2017). Extracellular vesicles isolated from the leaf apoplast carry stress-response proteins. Plant Physiol. 173 (1), 728–741. Epub 2016 Nov 8. PMID: 27837092; PMCID: PMC5210723. See on: Publisher's pub med |Google Scholar. 10.1104/pp.16.01253.

30. He, B. , Cai, Q. , Qiao, L. , Huang, C.-Y. , Wang, S. , Miao, W. , Ha, T. , Wang, Y. , & Jin, H. (2021). RNA-binding proteins contribute to small RNA loading in plant extracellular vesicles. Nature Plants, 7(3), 342–352.

31. Li A, Li D, Gu Y, Liu R, Tang X, Zhao Y, Qi F, Wei J, Liu J. Plant-derived nanovesicles: Further exploration of biomedical function and application potential. Acta Pharm Sin B. 2023 Aug;13(8):3300-3320. doi: 10.1016/j.apsb.2022.12.022. Epub 2023 Mar 7. PMID: 37655320; PMCID: PMC10465964.

32. Cao, M., Yan, H., Han, X., Weng, L., Wei, Q., Sun, X., Lu, W., Wei, Q., Ye, J., Cai, X. and Hu, C., 2019. Ginseng-derived nanoparticles alter macrophage polarization to inhibit melanoma growth. Journal for immunotherapy of cancer, 7, pp.1-18.

33. Karamanidou T, Tsouknidas A. Plant-Derived Extracellular Vesicles as Therapeutic Nanocarriers. Int J Mol Sci. 2021 Dec 24;23(1):191. doi: 10.3390/ijms23010191. PMID: 35008617; PMCID: PMC8745116.

34. Pocsfalvi, G., Turiák, L., Ambrosone, A., Del Gaudio, P., Puska, G., Fiume, I., Silvestre, T. and Vékey, K., 2018. Protein biocargo of citrus fruit-derived vesicles reveals heterogeneous transport and extracellular vesicle populations. Journal of plant physiology, 229, pp.111-121.

35. Chin AR, Fong MY, Somlo G, Wu J, Swiderski P, Wu X, Wang SE. Cross-kingdom inhibition of breast cancer growth by plant miR159. Cell Res. 2016 Feb;26(2):217-28. doi: 10.1038/cr.2016.13. Epub 2016 Jan 22. PMID: 26794868; PMCID: PMC4746606.

36. Potesta, M.; Roglia, V.; Fanelli, M.; Pietrobono, E.; Gismondi, A.; Vumbaca, S.; Nguedia Tsangueu, R.G.; Canini, A.; Colizzi, V.; Grelli, S.; et al. Effect of microvesicles from moringa oleifera containing mirna on proliferation and apoptosis in tumor cell lines.

37. Cell Death Discov. 2020, 6, 43.Yang M, Luo Q, Chen X, Chen F. Bitter melon derived extracellular vesicles enhance the therapeutic effects and reduce the drug resistance of 5-fluorouracil on oral squamous cell carcinoma. J Nanobiotechnology. 2021 Aug 28;19(1):259. doi: 10.1186/s12951-021-00995-1. PMID: 34454534; PMCID: PMC8400897.

38. Raimondo S, Naselli F, Fontana S, Monteleone F, Lo Dico A, Saieva L, Zito G, Flugy A, Manno M, Di Bella MA, De Leo G, Alessandro R. Citrus limon-derived nanovesicles inhibit cancer cell proliferation and suppress CML xenograft growth by inducing TRAIL-mediated cell death. Oncotarget. 2015 Aug 14;6(23):19514-27. doi: 10.18632/oncotarget.4004. PMID: 26098775; PMCID: PMC4637302.

39. Kalarikkal SP, Sundaram GM. Edible plant-derived exosomal microRNAs: Exploiting a cross-kingdom regulatory mechanism for targeting SARS-CoV-2. Toxicol Appl Pharmacol. 2021 Mar 1;414:115425. doi: 10.1016/j.taap.2021.115425. Epub 2021 Jan 29. PMID: 33516820; PMCID: PMC7844364.

40. Wang B, Zhuang X, Deng ZB, Jiang H, Mu J, Wang Q, Xiang X, Guo H, Zhang L, Dryden G, Yan J, Miller D, Zhang HG. Targeted drug delivery to intestinal macrophages by bioactive nanovesicles released from grapefruit. Mol Ther. 2014 Mar;22(3):522-534. doi: 10.1038/mt.2013.190. Epub 2013 Aug 13. PMID: 23939022; PMCID: PMC3944329.

41. Deng Z, Rong Y, Teng Y, Mu J, Zhuang X, Tseng M, Samykutty A, Zhang L, Yan J, Miller D, Suttles J, Zhang HG. Broccoli-Derived Nanoparticle Inhibits Mouse Colitis by Activating Dendritic Cell AMP-Activated Protein Kinase. Mol Ther. 2017 Jul 5;25(7):1641-1654. doi: 10.1016/j.ymthe.2017.01.025. Epub 2017 Mar 6. PMID: 28274798; PMCID: PMC5498816.

42. Raimondo S, Urzì O, Meraviglia S, Di Simone M, Corsale AM, Rabienezhad Ganji N, Palumbo Piccionello A, Polito G, Lo Presti E, Dieli F, Conigliaro A, Alessandro R. Anti-inflammatory properties of lemon-derived extracellular vesicles are achieved through the inhibition of ERK/NF-κB signalling pathways. J Cell Mol Med. 2022 Aug;26(15):4195-4209. doi: 10.1111/jcmm.17404. Epub 2022 Jul 4. PMID: 35789531; PMCID: PMC9344827.

43. Lugrin J, Rosenblatt-Velin N, Parapanov R, Liaudet L. The role of oxidative stress during inflammatory processes. Biol Chem. 2014 Feb;395(2):203-30. doi: 10.1515/hsz-2013-0241. PMID: 24127541.

44. Urzì O, Cafora M, Ganji NR, Tinnirello V, Gasparro R, Raccosta S, Manno M, Corsale AM, Conigliaro A, Pistocchi A, Raimondo S, Alessandro R. Lemon-derived nanovesicles achieve antioxidant and anti-inflammatory effects activating the AhR/Nrf2 signaling pathway. iScience. 2023 Jun 7;26(7):107041. doi: 10.1016/j.isci.2023.107041. PMID: 37426343; PMCID: PMC10329147.

45. Şahin F, Koçak P, Güneş MY, Özkan İ, Yıldırım E, Kala EY. In Vitro Wound Healing Activity of Wheat-Derived Nanovesicles. Appl Biochem Biotechnol. 2019 Jun;188(2):381-394. doi: 10.1007/s12010-018-2913-1. Epub 2018 Nov 26. PMID: 30474796.

46. Savcı Y, Kırbaş OK, Bozkurt BT, Abdik EA, Taşlı PN, Şahin F, Abdik H. Grapefruit-derived extracellular vesicles as a promising cell-free therapeutic tool for wound healing. Food Funct. 2021 Jun 8;12(11):5144-5156. doi: 10.1039/d0fo02953j. PMID: 33977960.

47. Younis M.A., Tawfeek H.M., Abdellatif A.A.H., Abdel-Aleem J.A., Harashima H. Clinical translation of nanomedicines: Challenges, opportunities, and keys. Adv. Drug Deliv. Rev. 2022;181:114083. doi: 10.1016/j.addr.2021.114083.

48. Schirrmacher V. From chemotherapy to biological therapy: A review of novel concepts to reduce the side effects of systemic cancer treatment (review) Int. J. Oncol. 2019;54:407–419. doi: 10.3892/ijo.2018.4661.

49. van der Meel R., Fens M.H., Vader P., van Solinge W.W., Eniola-Adefeso O., Schiffelers R.M. Extracellular vesicles as drug delivery systems: Lessons from the liposome field. J. Control Release. 2014;195:72–85. doi: 10.1016/j.jconrel.2014.07.049.

50. Paunovska K., Loughrey D., Dahlman J.E. Drug delivery systems for RNA therapeutics. Nat. Rev. Genet. 2022;23:265–280. doi: 10.1038/s41576-021-00439-4.

51. Barenholz Y. Doxil(r)—The first fda-approved nano-drug: Lessons learned. J. Control Release. 2012;160:117–134. doi: 10.1016/j.jconrel.2012.03.020.

52. Bulbake U., Doppalapudi S., Kommineni N., Khan W. Liposomal formulations in clinical use: An updated review. Pharmaceutics. 2017;9:12. doi: 10.3390/pharmaceutics9020012.

53. Colombo M., Raposo G., Thery C. Biogenesis, secretion, and intercellular interactions of exosomes and other extracellular vesicles. Annu. Rev. Cell Dev. Biol. 2014;30:255–289. doi: 10.1146/annurev-cellbio-101512-122326.

54. O'Brien K., Breyne K., Ughetto S., Laurent L.C., Breakefield X.O. Rna delivery by extracellular vesicles in mammalian cells and its applications. Nat. Rev. Mol. Cell Biol. 2020;21:585–606. doi: 10.1038/s41580-020-0251-y.

55. Valadi H., Ekstrom K., Bossios A., Sjostrand M., Lee J.J., Lotvall J.O. Exosome-mediated transfer of mrnas and micrornas is a novel mechanism of genetic exchange between cells. Nat. Cell Biol. 2007;9:654–659. doi: 10.1038/ncb1596.

56. Bonsergent E., Grisard E., Buchrieser J., Schwartz O., Thery C., Lavieu G. Quantitative characterization of extracellular vesicle uptake and content delivery within mammalian cells. Nat. Commun. 2021;12:1864. doi: 10.1038/s41467-021-22126-y.
57. Elsharkasy O.M., Nordin J.Z., Hagey D.W., de Jong O.G., Schiffelers R.M., Andaloussi S.E., Vader P. Extracellular vesicles as drug delivery systems: Why and how? Adv. Drug Deliv. Rev. 2020;159:332–343. doi: 10.1016/j.addr.2020.04.004.
58. Witwer KW, Wolfram J. Extracellular vesicles versus synthetic nanoparticles for drug delivery. Nat Rev Mater. 2021 Feb;6(2):103-106. doi: 10.1038/s41578-020-00277-6. Epub 2021 Jan 7. PMID: 36117545; PMCID: PMC9481198.
59. Rabienezhad Ganji N, Urzì O, Tinnirello V, Costanzo E, Polito G, Palumbo Piccionello A, Manno M, Raccosta S, Gallo A, Lo Pinto M, Calligaris M, Scilabra SD, Di Bella MA, Conigliaro A, Fontana S, Raimondo S, Alessandro R. Proof-of-Concept Study on the Use of Tangerine-Derived Nanovesicles as siRNA Delivery Vehicles toward Colorectal Cancer Cell Line SW480. Int J Mol Sci. 2023 Dec 30;25(1):546. doi: 10.3390/ijms25010546. PMID: 38203716; PMCID: PMC10779162.
60. Deng W, Meng Y, Wang B, Wang CX, Hou CX, Zhu QH, Tang YT, Ye JH. In vitro experimental study on the formation of microRNA-34a loaded exosomes and their inhibitory effect in oral squamous cell carcinoma. Cell Cycle. 2022 Aug;21(16):1775-1783. doi: 10.1080/15384101.2022.2070832. Epub 2022 Apr 29. PMID: 35485349; PMCID: PMC9302529.
61. Didiot MC, Hall LM, Coles AH, Haraszti RA, Godinho BM, Chase K, Sapp E, Ly S, Alterman JF, Hassler MR, Echeverria D, Raj L, Morrissey DV, DiFiglia M, Aronin N, Khvorova A. Exosome-mediated Delivery of Hydrophobically Modified siRNA for Huntingtin mRNA Silencing. Mol Ther. 2016 Oct;24(10):1836-1847. doi: 10.1038/mt.2016.126. Epub 2016 Jun 27. PMID: 27506293; PMCID: PMC5112038.
62. Hettich B.F., Bader J.J., Leroux J.C. Encapsulation of hydrophilic compounds in small extracellular vesicles: Loading capacity and impact on vesicle functions. Adv. Healthc. Mater. 2022;11:e2100047. doi: 10.1002/adhm.202100047.
63. Gehl J. Electroporation: Theory and methods, perspectives for drug delivery, gene therapy and research. Acta Physiol. Scand. 2003;177:437–447. doi: 10.1046/j.1365-201X.2003.01093.x.
64. Tian Y., Li S., Song J., Ji T., Zhu M., Anderson G.J., Wei J., Nie G. A doxorubicin delivery platform using engineered natural membrane vesicle exosomes for targeted tumor therapy. Biomaterials. 2014;35:2383–2390. doi: 10.1016/j.biomaterials.2013.11.083.
65. Hood J.L., Scott M.J., Wickline S.A. Maximizing exosome colloidal stability following electroporation. Anal. Biochem. 2014;448:41–49. doi: 10.1016/j.ab.2013.12.001.
66. Haney M.J., Klyachko N.L., Harrison E.B., Zhao Y., Kabanov A.V., Batrakova E.V. Tpp1 delivery to lysosomes with extracellular vesicles and their enhanced brain distribution in the animal model of batten disease. Adv. Healthc. Mater. 2019;8:e1801271. doi: 10.1002/adhm.201801271.

67. Salarpour S, Forootanfar H, Pournamdari M, Ahmadi-Zeidabadi M, Esmaeeli M, Pardakhty A. Paclitaxel incorporated exosomes derived from glioblastoma cells: comparative study of two loading techniques. Daru. 2019 Dec;27(2):533-539. doi: 10.1007/s40199-019-00280-5. Epub 2019 Jul 17. PMID: 31317441; PMCID: PMC6895332.

68. Wan Z, Zhao L, Lu F, Gao X, Dong Y, Zhao Y, Wei M, Yang G, Xing C, Liu L. Mononuclear phagocyte system blockade improves therapeutic exosome delivery to the myocardium. Theranostics. 2020 Jan 1;10(1):218-230. doi: 10.7150/thno.38198. PMID: 31903116; PMCID: PMC6929612.

69. Del Pozo-Acebo L., Lopez de Las Hazas M.C., Tome-Carneiro J., Del Saz-Lara A., Gil-Zamorano J., Balaguer L., Chapado L.A., Busto R., Visioli F., Davalos A. Therapeutic potential of broccoli-derived extracellular vesicles as nanocarriers of exogenous mirnas. Pharmacol. Res. 2022;185:106472. doi: 10.1016/j.phrs.2022.106472.

70. You J.Y., Kang S.J., Rhee W.J. Isolation of cabbage exosome-like nanovesicles and investigation of their biological activities in human cells. Bioact. Mater. 2021;6:4321–4332. doi: 10.1016/j.bioactmat.2021.04.023.

71. Xi XM, Xia SJ, Lu R. Drug loading techniques for exosome-based drug delivery systems. Pharmazie. 2021 Feb 25;76(2):61-67. doi: 10.1691/ph.2021.0128. PMID: 33714281.

72. Han Y, Jones TW, Dutta S, Zhu Y, Wang X, Narayanan SP, Fagan SC, Zhang D. Overview and Update on Methods for Cargo Loading into Extracellular Vesicles. Processes (Basel). 2021 Feb;9(2):356. doi: 10.3390/pr9020356. Epub 2021 Feb 15. PMID: 33954091; PMCID: PMC8096148.

73. Alvarez-Erviti L, Seow Y, Yin H, Betts C, Lakhal S, Wood MJ. Delivery of siRNA to the mouse brain by systemic injection of targeted exosomes. Nat Biotechnol. 2011 Apr;29(4):341-5. doi: 10.1038/nbt.1807. Epub 2011 Mar 20. PMID: 21423189.

74. Faruqu FN, Xu L, Al-Jamal KT. Preparation of Exosomes for siRNA Delivery to Cancer Cells. J Vis Exp. 2018 Dec 5;(142):10.3791/58814. doi: 10.3791/58814. PMID: 30582600; PMCID: PMC6785346.

75. Urzì O, Gasparro R, Ganji NR, Alessandro R, Raimondo S. Plant-RNA in Extracellular Vesicles: The Secret of Cross-Kingdom Communication. Membranes (Basel). 2022 Mar 23;12(4):352. doi: 10.3390/membranes12040352. PMID: 35448322; PMCID: PMC9028404.

76. Zhang Z, Yu Y, Zhu G, Zeng L, Xu S, Cheng H, Ouyang Z, Chen J, Pathak JL, Wu L, Yu L. The Emerging Role of Plant-Derived Exosomes-Like Nanoparticles in Immune Regulation and Periodontitis Treatment. Front Immunol. 2022 Jun 10;13:896745. doi: 10.3389/fimmu.2022.896745. PMID: 35757759; PMCID: PMC9231591.

77. Cui Y, Gao J, He Y, Jiang L. Plant extracellular vesicles. Protoplasma. 2020 Jan;257(1):3-12. doi: 10.1007/s00709-019-01435-6. Epub 2019 Aug 30. PMID: 31468195.

78. Li Z, Wang H, Yin H, Bennett C, Zhang HG, Guo P. Arrowtail RNA for Ligand Display on Ginger Exosome-like Nanovesicles to Systemic Deliver siRNA for Cancer Suppression. Sci Rep. 2018 Oct 2;8(1):14644. doi: 10.1038/s41598-018-32953-7. PMID: 30279553; PMCID: PMC6168523.

79. Raimondo S, Cristaldi M, Fontana S, Saieva L, Monteleone F, Calabrese G, Giavaresi G, Parenti R, Alessandro R. The phospholipase DDHD1 as a new target in colorectal cancer therapy. J Exp Clin Cancer Res. 2018 Apr 13;37(1):82. doi: 10.1186/s13046-018-0753-z. PMID: 29653539; PMCID: PMC5899352.
80. Dorfmüller, T. B. J. Berne and r. Pecora: Dynamic light scattering, john wiley and sons ltd., baffins lane 1976, 376 seiten, preis: £ 14,—. Berichte der Bunsengesellschaft für physikalische Chemie 1977, 81, 101-101. https://doi.org/10.1002/pi.4980090216.
81. Adamo G, Fierli D, Romancino DP, Picciotto S, Barone ME, et al., Manno M, Bongiovanni A. Nanoalgosomes: Introducing extracellular vesicles produced by microalgae. J Extracell Vesicles. 2021 Apr;10(6):e12081. doi: 10.1002/jev2.12081. Epub 2021 Apr 27. PMID: 33936568; PMCID: PMC8077145.
82. Paterna A, Rao E, Adamo G, Raccosta S, Picciotto S, Romancino D, Noto R, Touzet N, Bongiovanni A, Manno M. Isolation of Extracellular Vesicles From Microalgae: A Renewable and Scalable Bioprocess. Front Bioeng Biotechnol. 2022 Mar 14;10:836747. doi: 10.3389/fbioe.2022.836747. PMID: 35360396; PMCID: PMC8963918.
83. Hutter, J.L.; Bechhoefer, J. Calibration of atomic-force microscope tips. Review of scientific instruments 1993, 64, 1868-1873.
84. Kıyga E, Adıgüzel Z, Önay Uçar E. Temozolomide increases heat shock proteins in extracellular vesicles released from glioblastoma cells. Mol Biol Rep. 2022 Sep;49(9):8701-8713. doi: 10.1007/s11033-022-07714-5. Epub 2022 Jun 25. PMID: 35752701.
85. Andreu Z, Yáñez-Mó M. Tetraspanins in extracellular vesicle formation and function. Front Immunol. 2014 Sep 16;5:442. doi: 10.3389/fimmu.2014.00442. PMID: 25278937; PMCID: PMC4165315.
86. Wu Q, Wei H, Meng W, Xie X, Zhang Z, Su G. Effect of AnnexinA Group Translocated in Extracellular Vesicles on Tumorigenesis. Curr Mol Med. 2021;21(4):347-353. doi: 10.2174/1566524020666200825163512. PMID: 32842939.
87. Bucci-Muñoz M, Gola AM, Rigalli JP, Ceballos MP, Ruiz ML. Extracellular Vesicles and Cancer Multidrug Resistance: Undesirable Intercellular Messengers? Life (Basel). 2023 Jul 27;13(8):1633. doi: 10.3390/life13081633. PMID: 37629489; PMCID: PMC10455762.
88. Das P, Mukherjee A, Adak S. Glyceraldehyde-3-phosphate dehydrogenase present in extracellular vesicles from Leishmania major suppresses host TNF-alpha expression. J Biol Chem. 2021 Oct;297(4):101198. doi: 10.1016/j.jbc.2021.101198. Epub 2021 Sep 15. PMID: 34534548; PMCID: PMC8502904.
89. Zhang M, Xie Y, Li S, Ye X, Jiang Y, Tang L, Wang J. Proteomics Analysis of Exosomes From Patients With Active Tuberculosis Reveals Infection Profiles and Potential Biomarkers. Front Microbiol. 2022 Jan 6;12:800807. doi: 10.3389/fmicb.2021.800807. PMID: 35069505; PMCID: PMC8770970.
90. Kim MS, Haney MJ, Zhao Y, Mahajan V, Deygen I, Klyachko NL, Inskoe E, Piroyan A, Sokolsky M, Okolie O, Hingtgen SD, Kabanov AV, Batrakova EV. Development of exosome-encapsulated

paclitaxel to overcome MDR in cancer cells. Nanomedicine. 2016 Apr;12(3):655-664. doi: 10.1016/j.nano.2015.10.012. Epub 2015 Nov 14. PMID: 26586551; PMCID: PMC4809755.

91. Christensen J, El-Gebali S, Natoli M, Sengstag T, Delorenzi M, Bentz S, Bouzourene H, Rumbo M, Felsani A, Siissalo S, Hirvonen J, Vila MR, Saletti P, Aguet M, Anderle P. Defining new criteria for selection of cell-based intestinal models using publicly available databases. BMC Genomics. 2012 Jun 22;13:274. doi: 10.1186/1471-2164-13-274. PMID: 22726358; PMCID: PMC3412164.

92. Wang Q, Zhuang X, Mu J, Deng ZB, Jiang H, Zhang L, Xiang X, Wang B, Yan J, Miller D, Zhang HG. Delivery of therapeutic agents by nanoparticles made of grapefruit-derived lipids. Nat Commun. 2013;4:1867. doi: 10.1038/ncomms2886. Erratum in: Nat Commun. 2013;4:2358. Zhang, Lifeng [added]. Erratum in: Nat Commun. 2016;7:11347. PMID: 23695661; PMCID: PMC4396627.

93. Wang Q, Ren Y, Mu J, Egilmez NK, Zhuang X, Deng Z, Zhang L, Yan J, Miller D, Zhang HG. Grapefruit-Derived Nanovectors Use an Activated Leukocyte Trafficking Pathway to Deliver Therapeutic Agents to Inflammatory Tumor Sites. Cancer Res. 2015 Jun 15;75(12):2520-9. doi: 10.1158/0008-5472.CAN-14-3095. Epub 2015 Apr 16. Erratum in: Cancer Res. 2016 May 1;76(9):2845. PMID: 25883092; PMCID: PMC4470740.

94. Zhuang X, Teng Y, Samykutty A, Mu J, Deng Z, Zhang L, Cao P, Rong Y, Yan J, Miller D, Zhang HG. Grapefruit-derived Nanovectors Delivering Therapeutic miR17 Through an Intranasal Route Inhibit Brain Tumor Progression. Mol Ther. 2016 Feb;24(1):96-105. doi: 10.1038/mt.2015.188. Epub 2015 Oct 7. PMID: 26444082; PMCID: PMC4754550.

95. Zhuang X, Deng ZB, Mu J, Zhang L, Yan J, Miller D, Feng W, McClain CJ, Zhang HG. Ginger-derived nanoparticles protect against alcohol-induced liver damage. J Extracell Vesicles. 2015 Nov 25;4:28713. doi: 10.3402/jev.v4.28713. PMID: 26610593; PMCID: PMC4662062.

96. Teng Y, Mu J, Hu X, Samykutty A, Zhuang X, Deng Z, Zhang L, Cao P, Yan J, Miller D, Zhang HG. Grapefruit-derived nanovectors deliver miR-18a for treatment of liver metastasis of colon cancer by induction of M1 macrophages. Oncotarget. 2016 May 3;7(18):25683-97. doi: 10.18632/oncotarget.8361. PMID: 27028860; PMCID: PMC5041936.

97. Xiao Q, Zhao W, Wu C, Wang X, Chen J, Shi X, Sha S, Li J, Liang X, Yang Y, Guo H, Wang Y, Fan JB. Lemon-Derived Extracellular Vesicles Nanodrugs Enable to Efficiently Overcome Cancer Multidrug Resistance by Endocytosis-Triggered Energy Dissipation and Energy Production Reduction. Adv Sci (Weinh). 2022 Jul;9(20):e2105274. doi: 10.1002/advs.202105274. Epub 2022 Feb 20. PMID: 35187842; PMCID: PMC9284146.

98. Garaeva L, Kamyshinsky R, Kil Y, Varfolomeeva E, Verlov N, Komarova E, Garmay Y, Landa S, Burdakov V, Myasnikov A, Vinnikov IA, Margulis B, Guzhova I, Kagansky A, Konevega AL, Shtam T. Delivery of functional exogenous proteins by plant-derived vesicles to human cells in vitro. Sci Rep. 2021 Mar 22;11(1):6489. doi: 10.1038/s41598-021-85833-y. PMID: 33753795; PMCID: PMC7985202.

99. Zhang M, Xiao B, Wang H, Han MK, Zhang Z, Viennois E, Xu C, Merlin D. Edible Ginger-derived Nano-lipids Loaded with Doxorubicin as a Novel Drug-delivery Approach for Colon Cancer Therapy.

Mol Ther. 2016 Oct;24(10):1783-1796. doi: 10.1038/mt.2016.159. Epub 2016 Aug 5. PMID: 27491931; PMCID: PMC5112046.

100. Arafa EA, Shurrab NT, Buabeid MA. Therapeutic Implications of a Polymethoxylated Flavone, Tangeretin, in the Management of Cancer via Modulation of Different Molecular Pathways. Adv Pharmacol Pharm Sci. 2021 Mar 5;2021:4709818. doi: 10.1155/2021/4709818. PMID: 33748757; PMCID: PMC7954633.

101. Mdkhana B, Zaher DM, Abdin SM, Omar HA. Tangeretin boosts the anticancer activity of metformin in breast cancer cells via curbing the energy production. Phytomedicine. 2021 Mar;83:153470. doi: 10.1016/j.phymed.2021.153470. Epub 2021 Jan 17. PMID: 33524703.

102. Abdel-Fattah MM, Mohamed WR, Hassanein EHM, Arab HA, Arafa EA. Role of NF-κB/ICAM-1, JAK/STAT-3, and apoptosis signaling in the anticancer effect of tangeretin against urethane-induced lung cancer in BALB/c mice. Life Sci. 2023 Jul 15;325:121749. doi: 10.1016/j.lfs.2023.121749. Epub 2023 May 2. PMID: 37142089.

103. Sohel M, Sultana H, Sultana T, Al Amin M, Aktar S, Ali MC, Rahim ZB, Hossain MA, Al Mamun A, Amin MN, Dash R. Chemotherapeutic potential of hesperetin for cancer treatment, with mechanistic insights: A comprehensive review. Heliyon. 2022 Jan 23;8(1):e08815. doi: 10.1016/j.heliyon.2022.e08815. PMID: 35128104; PMCID: PMC8810372.

104. Chen X, Wei W, Li Y, Huang J, Ci X. Hesperetin relieves cisplatin-induced acute kidney injury by mitigating oxidative stress, inflammation and apoptosis. Chem Biol Interact. 2019 Aug 1;308:269-278. doi: 10.1016/j.cbi.2019.05.040. Epub 2019 May 31. PMID: 31153982.

105. Nouri Z, Fakhri S, Nouri K, Wallace CE, Farzaei MH, Bishayee A. Targeting Multiple Signaling Pathways in Cancer: The Rutin Therapeutic Approach. Cancers (Basel). 2020 Aug 14;12(8):2276. doi: 10.3390/cancers12082276. PMID: 32823876; PMCID: PMC7463935.

106. Elsayed HE, Ebrahim HY, Mohyeldin MM, Siddique AB, Kamal AM, Haggag EG, El Sayed KA. Rutin as A Novel c-Met Inhibitory Lead for The Control of Triple Negative Breast Malignancies. Nutr Cancer. 2017 Nov-Dec;69(8):1256-1271. doi: 10.1080/01635581.2017.1367936. Epub 2017 Oct 30. PMID: 29083228; PMCID: PMC6193555.

107. Kim K, Yoo HJ, Jung JH, Lee R, Hyun JK, Park JH, Na D, Yeon JH. Cytotoxic Effects of Plant Sap-Derived Extracellular Vesicles on Various Tumor Cell Types. J Funct Biomater. 2020 Apr 2;11(2):22. doi: 10.3390/jfb11020022. PMID: 32252412; PMCID: PMC7353476.

108. Demirgan, R., Karagöz, A., Pekmez, M., Önay-Uçar, E., Artun, F. T., Gürer, Ç., & Mat, A. (2016). In vitro anticancer activity and cytotoxicity of some papaver alkaloids on cancer and normal cell lines. African Journal of Traditional, Complementary and Alternative Medicines, 13(3), 22-26.

109. Zeng L, Wang H, Shi W, Chen L, Chen T, Chen G, Wang W, Lan J, Huang Z, Zhang J, Chen J. Aloe derived nanovesicle as a functional carrier for indocyanine green encapsulation and phototherapy. J Nanobiotechnology. 2021 Dec 20;19(1):439. doi: 10.1186/s12951-021-01195-7. PMID: 34930289; PMCID: PMC8686546.

110. Umezu T, Takanashi M, Murakami Y, Ohno SI, Kanekura K, Sudo K, Nagamine K, Takeuchi S, Ochiya T, Kuroda M. Acerola exosome-like nanovesicles to systemically deliver nucleic acid medicine via oral administration. Mol Ther Methods Clin Dev. 2021 Mar 10;21:199-208. doi: 10.1016/j.omtm.2021.03.006. PMID: 33850951; PMCID: PMC8010214.

111. Zhang M, Wang X, Han MK, Collins JF, Merlin D. Oral administration of ginger-derived nanolipids loaded with siRNA as a novel approach for efficient siRNA drug delivery to treat ulcerative colitis. Nanomedicine (Lond). 2017 Aug;12(16):1927-1943. doi: 10.2217/nnm-2017-0196. Epub 2017 Jun 30. PMID: 28665164; PMCID: PMC5827822.

112. Woith E, Guerriero G, Hausman JF, Renaut J, Leclercq CC, Weise C, Legay S, Weng A, Melzig MF. Plant Extracellular Vesicles and Nanovesicles: Focus on Secondary Metabolites, Proteins and Lipids with Perspectives on Their Potential and Sources. Int J Mol Sci. 2021 Apr 2;22(7):3719. doi: 10.3390/ijms22073719. PMID: 33918442; PMCID: PMC8038311.

113. Pomatto MAC, Bussolati B, D'Antico S, Ghiotto S, Tetta C, Brizzi MF, Camussi G. Improved Loading of Plasma-Derived Extracellular Vesicles to Encapsulate Antitumor miRNAs. Mol Ther Methods Clin Dev. 2019 Jan 9;13:133-144. doi: 10.1016/j.omtm.2019.01.001. PMID: 30788382; PMCID: PMC6370572.

114. Lennaárd AJ, Mamand DR, Wiklander RJ, El Andaloussi S, Wiklander OPB. Optimised Electroporation for Loading of Extracellular Vesicles with Doxorubicin. Pharmaceutics. 2021 Dec 24;14(1):38. doi: 10.3390/pharmaceutics14010038. PMID: 35056933; PMCID: PMC8780628.

115. Zhan g B, Yang Y, Tao R, Yao C, Zhou Z, Zhang Y. Exosomes loaded with miR-665 inhibit the progression of osteosarcoma in vivo and in vitro. Am J Transl Res. 2022 Oct 15;14(10):7012-7026. PMID: 36398229; PMCID: PMC9641455.

116. Rong Y, Wang Z, Tang P, Wang J, Ji C, Chang J, Zhu Y, Ye W, Bai J, Liu W, Yin G, Yu L, Zhou X, Cai W. Engineered extracellular vesicles for delivery of siRNA promoting targeted repair of traumatic spinal cord injury. Bioact Mater. 2022 Nov 25;23:328-342. doi: 10.1016/j.bioactmat.2022.11.011. PMID: 36474657; PMCID: PMC9706413.

117. Liang G, Zhu Y, Ali DJ, Tian T, Xu H, Si K, Sun B, Chen B, Xiao Z. Engineered exosomes for targeted co-delivery of miR-21 inhibitor and chemotherapeutics to reverse drug resistance in colon cancer. J Nanobiotechnology. 2020 Jan 9;18(1):10. doi: 10.1186/s12951-019-0563-2. PMID: 31918721; PMCID: PMC6950820.

118. Minna E, Romeo P, De Cecco L, Dugo M, Cassinelli G, Pilotti S, Degl'Innocenti D, Lanzi C, Casalini P, Pierotti MA, Greco A, Borrello MG. miR-199a-3p displays tumor suppressor functions in papillary thyroid carcinoma. Oncotarget. 2014 May 15;5(9):2513-28. Doi: 10.18632/oncotarget.1830. PMID: 24810336; PMCID: PMC4058023.

119. Wu F, Lin X, Shan SK, Li F, Xu F, Zhong JY, Guo B, Zheng MH, Wang Y, Mo ZH, Yuan LQ. The Suppression of miR-199a-3p by Promoter Methylation Contributes to Papillary Thyroid Carcinoma

Aggressiveness by Targeting RAP2a and DNMT3a. Front Cell Dev Biol. 2020 Dec 7;8:594528. doi: 10.3389/fcell.2020.594528. PMID: 33365310; PMCID: PMC7750465.

120. Zhang X, Li D, Li M, Ye M, Ding L, Cai H, Fu D, Lv Z. MicroRNA-146a targets PRKCE to modulate papillary thyroid tumor development. Int J Cancer. 2014 Jan 15;134(2):257-67. doi: 10.1002/ijc.28141. Epub 2013 Sep 18. PMID: 23457043.

121. Ma HL, Jiang Q, Han S, Wu Y, Cui Tomshine J, Wang D, Gan Y, Zou G, Liang XJ. Multicellular tumor spheroids as an in vivo-like tumor model for three-dimensional imaging of chemotherapeutic and nano material cellular penetration. Mol Imaging. 2012 Nov-Dec;11(6):487-98. PMID: 23084249.

122. Lee MA, Bergdorf KN, Phifer CJ, Jones CY, Byon SY, Sawyer LM, Bauer JA, Weiss VL. Novel three-dimensional cultures provide insights into thyroid cancer behavior. Endocr Relat Cancer. 2020 Feb;27(2):111-121. doi: 10.1530/ERC-19-0374. PMID: 31804972; PMCID: PMC7295136.

Acknowledgements

Sono profondamente grato per il viaggio attraverso l'ampio campo della ricerca scientifica, un percorso disseminato di sfide che hanno plasmato la mia personalità accademica. La mia gratitudine più profonda si estende a tutti i miei compagni che mi hanno costantemente sostenuto e guidato lungo questo cammino, consentendomi di realizzare le mie aspirazioni. Desidero esprimere il mio sincero apprezzamento all'intero gruppo di ricerca della Sezione Bi.N.D per aver favorito un'atmosfera serena pervasa da energia positiva. Primo fra tutti, esprimo la mia più sincera gratitudine al Professor Riccardo Alessandro, il mio supervisore di progetto, il cui sostegno, guida e disponibilità negli ultimi tre anni sono stati fondamentali nel superare ogni ostacolo. Estendo il mio sincero ringraziamento alla Professoressa Fontana e Corrado per la loro costante attenzione, dedizione incrollabile e preziosa mentorship sul luogo di lavoro. Il loro costante sostegno e guida illuminante hanno giocato un ruolo cruciale nel plasmare il mio percorso accademico. Inoltre, estendo il mio sincero apprezzamento alla Professoressa Conigliaro per la sua gentilezza, incoraggiamento e guida incrollabile in tutti i miei sforzi accademici. La sua mentorship è stata un faro di luce, illuminando il mio cammino e promuovendo la mia crescita come ricercatore. Un ringraziamento speciale è riservato alla mia cara Stefania, la cui fiducia incrollabile è stata una fonte costante di motivazione. La sua paziente mentorship è stata preziosa e attribuisco una parte significativa del mio successo accademico alla sua dedizione e supporto. Sono molto grato a Marzia e Marilena per il loro prezioso aiuto durante vari esperimenti in laboratorio. La loro competenza e dedizione hanno contribuito in modo significativo al successo di questa ricerca. Sono grato ai miei cari amici di questi ultimi tre anni. Ornella, che mi ha guidato durante il mio addestramento iniziale, e Marta, Daragana e Liana, il vostro sostegno ha contribuito significativamente alla mia crescita accademica. Anche se la vostra assenza si è fatta sentire nell'ultimo anno, i ricordi condivisi rimangono preziosi. A Vichi, Roberta e alla gentile Giulia, è stato un grande onore collaborare con individui così dedicati e ispiratori come voi. Insieme, abbiamo formato un gruppo coeso, diligente e laborioso, e sono profondamente grato per il vostro costante sostegno che mi avete esteso lungo il nostro percorso condiviso. Il vostro incoraggiamento e assistenza sono stati indispensabili e senza il vostro sostegno costante, navigare in questo percorso sarebbe stato indubbiamente molto più difficile. A Elisa, Marco, Aurora, e Chiara anche se i nostri progetti hanno seguito traiettorie diverse, la profondità del vostro sincero sostegno e incoraggiamento ha profondamente influenzato il mio cammino. La vostra incrollabile fiducia in me, unita alla vostra disponibilità a tendere una mano quando necessario, ha lasciato un segno indelebile sulla mia crescita accademica e personale. Sono profondamente grato per la vostra amicizia e sostegno, che hanno arricchito il mio percorso in modi innumerevoli. Sono grato al gruppo presso l'IOR - Daniele, Angela, Lavinia e Viviana - per la vostra pazienza e assistenza con ogni richiesta sul posto di lavoro. Estendo il nostro più sincero ringraziamento a tutti gli studenti magistrali il cui impegno e collaborazione hanno arricchito la nostra esperienza in laboratorio. Insieme, abbiamo condiviso non solo la ricerca scientifica, ma anche momenti di cameratismo e supporto, rendendo il nostro viaggio memorabile. Come studente di nazionalità persiana, sono profondamente toccato dal sostegno incrollabile della mia seconda famiglia in Italia, che mi ha trattato con il massimo rispetto e è

stata una costante fonte di supporto, sia accademico che personale. Esprimo la mia gratitudine al mio supervisore del Corso di Laurea magistrale in Iran, il Professor Ahmadi, la cui guida e ispirazione hanno acceso la mia passione per la ricerca scientifica e mi hanno condotto in questo viaggio trasformativo. Nel riconoscere la natura multifacetica della vita di un ricercatore, che comprende sia la ricerca accademica che i legami familiari, mi trovo di fronte alla sfida di trasmettere sufficientemente il mio apprezzamento a due figure chiave. In primo luogo, sono profondamente indebitato alla mia gentile Fatemeh, il cui sostegno incrollabile è stato un pilastro di forza, fornendo conforto e incoraggiamento nei momenti più difficili. La sua presenza nutritiva è stata una costante fonte di rassicurazione, guidandomi attraverso le complessità dell'accademia con compassione e comprensione. Allo stesso modo, sono profondamente grato al mio caro Rayan, la cui presenza è una fonte di motivazione e ispirazione. Insieme, Fatemeh e Rayan hanno svolto ruoli fondamentali nel plasmare il mio percorso e per il loro costante sostegno, sono eternamente grato. Dedico questa posizione e questo successo, specialmente ai miei genitori, il cui sostegno incrollabile, amore infinito e sacrifici instancabili sono stati la pietra angolare della mia speranza, forza e scopo nella vita. La loro guida e incoraggiamento mi hanno plasmato nella persona che sono oggi e sono eternamente grato per la loro incrollabile fiducia in me. Infine, estendo i miei più sentiti ringraziamenti ai miei amati fratelli e sorelle, la cui presenza mi manca profondamente. Auguro loro un continuo successo e realizzazione in tutti i loro sforzi, sapendo che il loro sostegno è stato una fonte di forza e ispirazione lungo tutto il mio percorso.